Quantum Electronics **37** (7) 605 – 622 (2007)

INVITED PAPER

PACS numbers: 42.65.An; 42.65.Jx; 42.70.Qs
DOI: 10.1070/QE2007v037n07ABEH013367

Nonlinear-optical parameters of various media

R.A. Ganeev, T. Usmanov

***Abstract*. A review of investigations of nonlinear refraction and nonlinear absorption of light in semiconductors, fullerenes, dyes, metals, and crystals is given. The results of measurements of the nonlinear refraction coefficients, nonlinear absorption coefficients, saturation intensities, and nonlinear susceptibilities of these media by using laser radiation at different wavelengths and the *z*-scan method are presented. Methods of preparation of nanoparticles based on these media and studies of their nonlinear-optical parameters are discussed. Some media are analysed from the point of view of their application as optical limiters of laser radiation. Investigations of higher nonlinearities of some media are also considered.**

Keywords: *nonlinear refraction, nonlinear absorption, z-scan.*

1. Introduction

The third-order nonlinear optical susceptibilities of various media change in a broad range from 10^{-17} cgs units to a few cgs units. Nonlinearities responsible for variations in the refractive and absorbing properties are especially important because they strongly affect the propagation of intense radiation in media. Numerous investigations have been performed in this field due to increasing interest in applications of nonlinear-optical effects in optoelectronics, various nonlinear optical devices, optical switching, etc. [1 – 3].

Interest in nonlinearities of different nanostructure media is also caused by their strong nonlinear-optical response caused by the quantum size effect. The application of nanostructures in the above-mentioned fields and optical computers, storage devices, nonlinear spectroscopy, etc. can lead to considerable development of the latter.

We present here a review of investigations of nonlinear-optical parameters of semiconductors, fullerenes, dyes, metals, and crystals in various spectral regions. Some of these media are analysed from the point of view of their use as optical limiters of the laser radiation intensity. The results of measurements of nonlinear refractive indices γ, nonlinear absorption coefficients β, and third-order nonlinear susceptibilities $\chi^{(3)}$ of these media are presented. The higher-order nonlinear susceptibilities of some materials are also analysed.

R.A. Ganeev, T. Usmanov Akadempribor Research and Production Association, Academy of Sciences of Uzbekistan, Akademgorodok, 700125 Tashkent; e-mail: lvliv@tps.uz

Received 16 August 2006; revision received 14 February 2007
Kvantovaya Elektronika **37** (7) 605 – 622 (2007)
Translated by M.N. Sapozhnikov

2. Analysis of nonlinear-optical parameters of media by the *z*-scan method

The nonlinear response of media can be measured by different methods such as nonlinear interferometry, three- and four-wave mixing, generation of harmonics, polarisation-ellipse rotation, probe-beam method, and analysis of distortions of the beam amplitude – phase profile [4 – 7]. However, most of these methods cannot provide the separation of contributions from different nonlinearities. One of the methods that can do it is the *z*-scan method, which is comparatively simple and provides high measurement accuracy [8]. At present, there exist several variants of this method: two-colour, shadow, reflection, and autocorrelation *z*-scan [9 – 11]. The nonlinear-optical response is calculated by microscopic and empirical methods [12 – 14].

The single-beam *z*-scan method [8, 11] is comparatively simple and offers a number of advantages over interferometric and other methods [6, 7]. In [8], a new highly sensitive single-beam method for measuring the nonlinear refractive index and nonlinear absorption coefficient of media was proposed. The method is based on the analysis of variations in the far-field intensity distribution of a laser beam caused by the nonlinear refraction of a sample displaced in the focal region along the laser beam direction (the *z* axis in Fig. 1). To explain the principle of the *z*-scan method, we consider the propagation of focused intense laser radiation through a medium under study. Consider nonlinear refraction and assume that the medium gives a positive nonlinear addition to the refractive index. If the sample is located at a large distance from the focus (the region of negative values of *z*), the radiation intensity in the medium is insufficient to excite a noticeable nonlinear refraction, and the transmission of radiation through an aperture mounted in the far-field zone remains invariable and close to unity, as shown in Fig. 2. As the sample approaches the focal point, the radiation intensity increases and the self-focusing effect appears in the medium. The beam-waist region is displaced to a lens (see solid straight lines behind the sample in Fig. 1a). As a result, the far-field radiation has a larger divergence and, hence, transmission through the limiting aperture decreases.

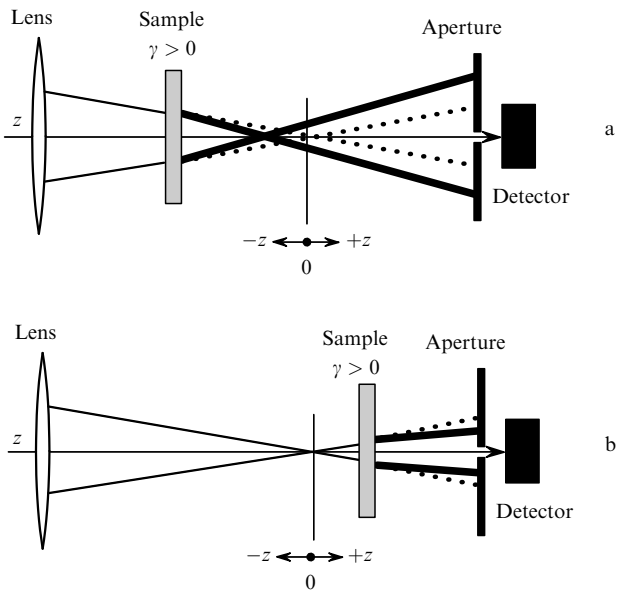

Figure 1. Schemes of propagation of focused intense radiation through a nonlinear self-focusing medium for a sample located in front of the focus (a) and behind it (b).

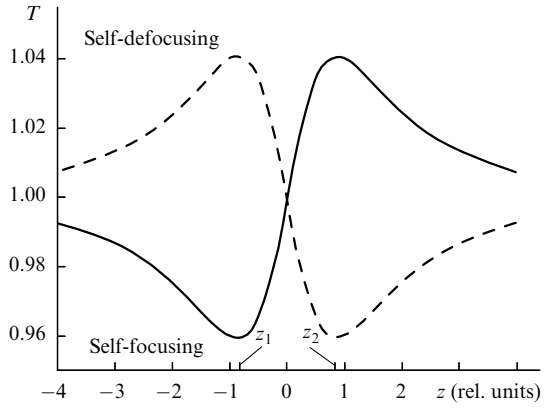

Figure 2. Normalised transmission in the limiting-aperture scheme for media with the positive (solid curve) and negative (dashed curve) nonlinear refractive indices.

As the sample is scanned along the z axis, transmission will decrease until the point z_1 is reached (see Fig. 2), where transmission is minimal. A decrease in the curvature of the wave front of a Gaussian beam near the focus causes the general decrease in the far-field radiation divergence, and as the sample further approaches the beam waist, transmission through the aperture increases. After the sample passes through the waist, the following picture is observed. Self-focusing reduces the far-field radiation divergence (see solid straight line behind the sample in Fig. 1b). This will continue until the influence of self-focusing on the radiation propagation through the aperture will be maximal (at the point z_2 in Fig. 2 corresponding to the maximum of the solid curve). As the sample is further displaced, the influence of this nonlinear-optical process on the transmission of radiation through the aperture will decrease because of the decrease in the radiation intensity until the normalised transmission achieves its stationary value close to unity. Thus, if the maximum of the normalised transmission follows after the minimum during z-scan, the medium has a positive nonlinear refractive index ($\gamma > 0$) and, on the contrary, if the transmission maximum first appears and then minimum, the medium has self-defocusing properties ($\gamma < 0$).

We considered above only one type of nonlinearity (nonlinear refraction), by neglecting the influence of nonlinearities producing variations in the absorptivity of the medium (such as multiphoton absorption and saturated absorption). The nonlinearity of the first type (multiphoton absorption) will lead to the suppression of the maximum and the increase in the dip depth in the dependence of the transmission $T(z)$ on the sample position. In the case of saturated absorption, the opposite picture will be observed. In the presence of both nonlinear-optical processes (nonlinear absorption and nonlinear refraction), we can separate the influence of one effect by subtraction methods and then calculate separately the nonlinear refractive index and nonlinear absorption coefficient. Moreover, taking into account that the z-scan method allows one to determine γ exclusively due to the presence of the limiting aperture, the removal of the latter completely eliminates the influence of self-focusing (self-defocusing) on the dependence $T(z)$. In this case, this scheme becomes sensitive only to nonlinear absorption. Therefore, the scheme with an open aperture can be used for measuring the nonlinear absorption coefficient.

We did not specify above the order of nonlinearity responsible for the nonlinear-optical process. Note that the influence of higher-order nonlinearities (for example, five-order nonlinear susceptibilities) becomes substantial for a number of media (in particular, semiconductors in which the appearance of free carriers due to two-photon absorption and their interaction with the intense field leads to the higher-order nonlinear response). In this case, the z-scan method also allows one to determine and separate the contributions of nonlinearities of different orders by the shape of the dependence $T(z)$ and positions of the transmission minimum and maximum.

It is known that under real experimental conditions, the precise measurement of the radiation intensity in the focal plane is a nontrivial task due to the difficulties encountered in the determination of its spatial parameters in a medium. Note in this connection an interesting feature of the dependence $T(z)$ described above. If nonlinear refraction is caused by the third-order nonlinearities, then for the sample length L smaller than the diffraction length z_0 of laser radiation, the distance Δz between the transmission maximum and minimum is related to the spatial characteristics of focused radiation in the focal plane by the expression [8]

$$\Delta z \simeq 1.7 z_0. \tag{1}$$

Here, $z_0 = 0.5 k w_0^2$; $k = 2\pi/\lambda$; w_0 is the beam radius at the $1/e^2$ level of the spatial intensity distribution in the focal plane; and λ is the radiation wavelength. Thus, the spatial parameters of focused radiation can be obtained with good accuracy from the dependence of the normalised transmission on z upon scanning the sample. This, in turn, allows one to calculate nonlinear-optical parameters with good accuracy.

Variations in the refractive index of a medium in the field of an electromagnetic wave, taking into account only the third-order nonlinearity, are determined by the relation

$$\Delta n(\omega) = \gamma(\omega) I_\omega = n_2(\omega) \frac{|E_\omega|^2}{2}, \quad (2)$$

where I_ω and E_ω are the intensity and strength of the electric field of the electromagnetic wave of frequency ω. The nonlinear refractive indices n_2 and γ, describing the same process in different measurement units, are related by the expression n_2 (in cgs units) $= (cn/40\pi)\gamma$ (in SI units), where n is the refractive index of the medium and c is the speed of light.

The value of γ is determined from z-scan experiments in the absence of nonlinear absorption by using the expression [8]

$$\Delta T = 0.404(1-S)^{0.25} \left| \frac{2\pi\gamma I_0 [1 - \exp(-\alpha L)]}{\alpha\lambda} \right|, \quad (3)$$

where ΔT is the normalised difference of the maximum and minimum transmission in the limiting-aperture scheme; I_0 is the maximum radiation intensity in the waist plane; S is the aperture transmission (fraction of radiation incident on a photocathode); and α is the linear absorption coefficient.

An important advantage of the z-scan method is the possibility to separate processes related to nonlinear absorption and nonlinear refraction when both these processes proceed simultaneously in a sample [6]. In this case, the theoretical dependence of the normalised transmission on z can be written in the form [15]

$$T(z) = 1 + \frac{4x}{(x^2+9)(x^2+1)} \Delta\Phi_0 - \frac{2(x^2+3)}{(x^2+9)(x^2+1)} \Delta\Psi_0, \quad (4)$$

where $x = z/z_0$; $\Delta\Phi_0 = k\gamma I_0 L_{\text{eff}}$, and $\Delta\Psi_0 = \beta I_0 L_{\text{eff}}/2$ are the parameters characterising the phase shift in the focus due to nonlinear refraction and nonlinear absorption, respectively; and $L_{\text{eff}} = [1 - \exp(-\alpha L)]/\alpha$ is the effective length of the sample. By introducing the notation $\rho = \beta/(2k\gamma)$, we can obtain the relation between $\Delta\Phi_0$ and $\Delta\Psi_0$ ($\Delta\Psi_0 = \rho\Delta\Phi_0$). In this case, the expression for the normalised transmission can be represented in the form

$$T = 1 + \frac{2(-\rho x^2 + 2x - 3\rho)}{(x^2+9)(x^2+1)} \Delta\Phi_0. \quad (5)$$

In the general case, the third-order nonlinear susceptibility is the complex quantity

$$\chi^{(3)} = \text{Re}\,\chi^{(3)} + \text{i}\,\text{Im}\,\chi^{(3)}. \quad (6)$$

Here, the imaginary part of nonlinearity is related to the nonlinear absorption coefficient by the expression

$$\text{Im}\,\chi^{(3)} = \frac{n^2 \varepsilon_0 c \lambda \beta}{2\pi}, \quad (7)$$

and the real part is caused by Kerr nonlinearities and is related to γ by the expression

$$\text{Re}\,\chi^{(3)} = 2n^2 \varepsilon_0 c \gamma, \quad (8)$$

where ε_0 is the dielectric constant. The value of $\chi^{(3)}$ in the cgs units is represented by the expression $\chi^{(3)}$ (in cgs units) $= (9 \times 10^8/4\pi)\chi^{(3)}$ (in SI units). The real part of the Kerr nonlinear susceptibility in the cgs units is related to the nonlinear refractive index by a simpler expression [16]

$$\chi^{(3)} = \frac{nn_2}{3\pi}. \quad (9)$$

Below, we describe the automated laser z-scan complex used for studying nonlinear-optical parameters of various media [17]. A picosecond Nd : YAG laser with a pulse repetition rate of 2 Hz was used in experiments. A single pulse of duration 35 or 55 ps was amplified up to the energy 2 mJ. Nonlinear-optical parameters were studied at the Nd:YAG laser radiation wavelength of 1064 nm and at the second- and third-harmonic wavelengths of 532 and 354.7 nm, respectively. Laser radiation was focused by lens (*1*) with a focal distance of 25 cm (Fig. 3). Objects (*2*) under study were displaced with the help of stage (*8*) along the optical axis z, by passing through the focal region. The system for sample translation included a micrometer drive and four-phase step motor (*7*) and provided a translation step of 20 μm per cycle. The focused-beam diameter in the waist region was 100 μm. In this case, the maximum radiation intensity was 4×10^{11} W cm^{-2} at 1064 nm, 4×10^{10} W cm^{-2} at 532 nm and 10^{10} W cm^{-2} at 354.7 nm and depended on the optical breakdown and multiphoton ionisation thresholds of media under study. The pulse-to-pulse energy fluctuations were ~10 %. The laser pulse energy was measured with calibrated FD-24K photodiode (*4*) and recorded with B9-5 stroboscopic voltage converter (*5*). The laser radiation energy was varied by using calibrated neutral filters.

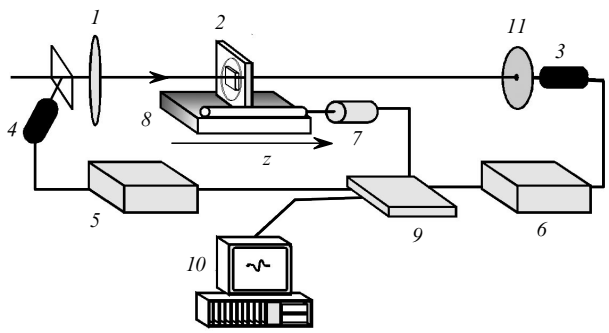

Figure 3. Scheme of an automated complex for measuring the nonlinear-optical parameters of various media [17]: (*1*) focusing lens; (*2*) sample; (*3*, *4*) photodiodes; (*5*, *6*) stroboscopic voltage converters; (*7*) four-phase step motor; (*8*) micro translation stage; (*9*) controller; (*10*) PC; (*11*) limiting aperture.

Aperture (*11*) of diameter 1 mm transmitting ~1 % of laser radiation was mounted at a distance of 150 cm from the focal region (the so-called limiting-aperture scheme). FD-24K photodiode (*3*) was mounted behind the aperture. The output signal of the photodiode was fed to B9-5 stroboscopic voltage converter (*6*). To eliminate the influence of instability of the output energy parameters of the laser on the results of measurements, the signal detected with photodiode (*3*) was normalised to the signal detected with second photodiode (*4*). The limiting-aperture scheme can be used to determine both the sign and values of γ and β

as well as the nonlinear susceptibility $\chi^{(3)}$ of materials. Nonlinear absorption can be also measured by using the so-called open-aperture scheme, when the aperture in the z-scan scheme is removed and all radiation transmitted by the sample upon its scanning along the z axis is collimated in photodiode (*3*). The expression for the normalised transmission in the open-aperture scheme has the form

$$T(z) = \frac{q^{-1}(z)}{\ln[1 + q(z)]}, \tag{10}$$

where

$$q(z) = \frac{\beta I(z) L_{\text{eff}}}{1 + (z_0^2/z^2)}.$$

The digitised output signals from both stroboscopic voltage converters were fed to controller (*9*) connected in series with PC (*10*). The results were processed by averaging measurements over the programmable number of points for the given coordinate z and rejecting individual measurements in the case of strong fluctuations on the incident radiation intensity. This reduces considerably the general measurement error of the sample transmission at the given point z. The measurement error was reduced by using a set of 20 individual measurements for a fixed position of the sample.

The measurements of the nonlinear refractive index were calibrated by using media with well-known nonlinear refractive indices (for example, quartz). Thus, the value of γ for quartz measured in our experiments was $(2.4 \pm 0.8) \times 10^{-16}$ cm^2 W^{-1}, in good agreement with the value 2×10^{-16} cm^2 W^{-1} obtained earlier [13]. The measurements of γ were calibrated similarly by using CS_2 [18].

3. Crystals

3.1 Photorefractive crystals

Investigations of higher-order nonlinear-optical processes in dielectric crystals involve certain problems due to the closeness of the optical breakdown and multiphoton ionisation thresholds to the intensities at which higher-order nonlinearities of these crystals are manifested [19–23]. Due to various applications of photorefractive media [24–31], such crystals as $Bi_{12}SiO_{20}$ (BSO), $Bi_{12}GeO_{20}$ (BGO), $Bi_{12}TiO_{20}$ (BTO), $BaTiO_3$, SBN, etc. attract considerable interest. To elucidate the potential possibilities of using photorefractive crystals, it is necessary to study in detail their optical and nonlinear-optical parameters. While these parameters in weak optical fields have been studied in many papers (see [24, 25] and references therein), the nonlinear-optical response of these crystals in the high-power IR field has been studied to a lesser degree at present [32–36]. In particular, picosecond radiation was used to study the efficiency and decay time of a diffraction grating induced in a BSO upon degenerate four-wave mixing. The self-focusing of the 457-nm laser radiation in photorefractive media was first observed in experiments with an SBN crystal [37].

Consider the results of z-scan investigations of self-focusing and other nonlinear-optical processes in photorefractive BSO and BGO crystals [38]. These crystals have large linear absorption coefficients n (2.55 and 2.44 for BSO and BGO, respectively) at a wavelength of 1064 nm. The z-scan experiments were performed by using 55-ps, 0.6-mJ pulses from a 1064-nm Nd:YAG laser and its second-harmonic 532-nm, 0.15-mJ pulses at a pulse repetition rate of 2 Hz. Figure 4 presents the dependence of the normalised transmission of the BSO crystal on z at 1064 nm in the limiting-aperture scheme. The nonlinear-optical parameters of BSO and BGO crystals measured at wavelengths of 1064 and 532 nm are presented in Table 1. According to the common practice accepted at present, the values of γ are presented in cm^2 W^{-1}, β – in cm W^{-1}, $\chi^{(3)}$, $\mathrm{Re}\,\chi^{(3)}$, and $\mathrm{Im}\,\chi^{(3)}$ – in the cgs units.

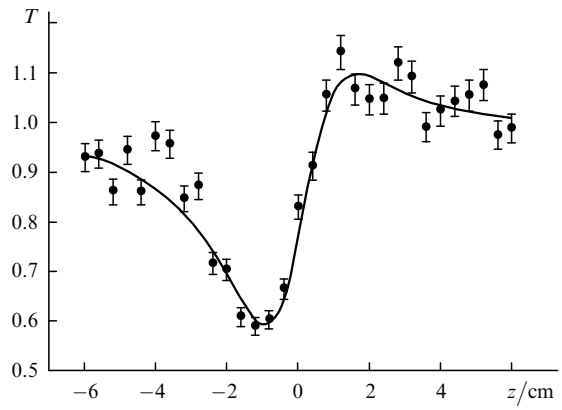

Figure 4. Dependences of the normalised transmission on the BSO crystal position (the ⟨110⟩ orientation) with respect to the focus in the limiting-aperture scheme. The solid curve is the theoretical dependence [38], circles are experiment.

Earlier [34], the generation of the conjugate wave in BSO and BGO crystals was treated as a result of considerable nonlinear absorption. The open-aperture z-scan study performed in [39] has demonstrated the presence of nonlinear absorption, which was the same within the experimental error for different orientations of BSO and BGO crystals. The type of nonlinear absorption was determined by analysing the width of the dip in the dependence of the normalised transmission on z.

In the case of a linear dependence on the intensity I, the absorption coefficient can be written in the form

$$\alpha(I) = \alpha_0 + \beta_{2\omega} I, \tag{11}$$

where α_0 is the intensity-independent linear absorption coefficient and $\beta_{2\omega}$ is the two-photon absorption coefficient. The theoretical dependence $T(z)$ calculated from (11) (dotted curve in Fig. 5) differs from the experimental dependence obtained by the open-aperture method. One can see that the experimental dip is narrower than the theoretical one. This discrepancy can be explained by assuming that higher-order nonlinear absorption processes (in particular, three-photon absorption) also take place.

The absorption spectra of BSO and BGO crystals show that the absorption edge related to impurities and crystal defects lies at 500 and 450 nm for these crystals, respectively. The energy gap width for these crystals is 3.2 eV. The ratio of the energy gap width to the Nd:YAG laser photon energy (1.17 eV) is equal to 2.7 for BSO and BGO. This circumstance considerably reduces the probability of two-photon absorption in these crystals at 1064 nm. Other

Table 1. Nonlinear-optical parameters of BSO and BGO crystals at 1064 and 532 nm [39].

Crystal	λ/mm	L/mm	$\gamma/10^{-14}$ cm^2 W^{-1}	Re $\chi^{(3)}/10^{-13}$ cgs units	$\beta_{2\omega}/10^{-9}$ cm W^{-1}	Im $\chi^{(3)}/10^{-13}$ cgs units	$\beta_{3\omega}/10^{-20}$ cm^3 W^{-2}
BSO	1064	10	0.4	1.6	–	–	2.5
			0.4	1.7	–	–	2.3
BGO		7.3	1	4.3	–	–	4.4
		11	1	4.3	–	–	4.2
		17	1	4.3	–	–	4.3
BSO	532	10	0.6	2.3	2	20	–
			0.7	3.0	1.6	17	–
BGO		7.3	1.2	5.1	3.7	38	–
		11	1.1	4.8	2.9	30	–
		17	1.2	5.1	3.6	38	–

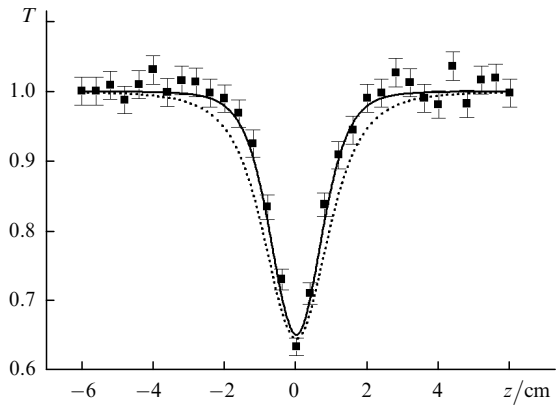

Figure 5. Dependences of the normalised transmission on the BGO crystal position with respect to the focus in the open-aperture scheme. The solid curve and dotted curves are theoretical dependences in the case of three- and two-photon absorption, respectively [39], squares are experiment.

possible higher-order mechanisms of nonlinear absorption were considered in [40]. In particular, taking three-photon absorption into account, the dependence of the absorption coefficient α on the intensity can be written in the form [41]

$$\alpha(I) = \alpha_0 + \beta_{2\omega} I + \beta_{3\omega} I^2, \tag{12}$$

where $\beta_{3\omega}$ is the three-photon absorption coefficient.

The theoretical dependence calculated by (12) is shown by the solid curve in Fig. 5. Good agreement with experimental data suggests that nonlinear absorption is related to three-photon processes. Table 1 presents three-photon absorption coefficients calculated from (12). Three-photon absorption coefficients measured in our experiments [$(2.5 \pm 0.8) \times 10^{-20}$ cm^3 W^{-2} for BSO and $(4.4 \pm 1.3) \times 10^{-20}$ cm^3 W^{-2} for BGO] are close to these coefficients measured for some materials at the same wavelength [in particular, $\beta_{3\omega} = (1.5 \pm 0.75) \times 10^{-20}$ cm^3 W^{-2} for CdS]. At the same time, these coefficients vary in a rather broad range depending on the medium (from 6.8×10^{-23} cm^3 W^{-2} for NaCl [19] to 2.0×10^{-19} cm^3 W^{-2} for InSb [23]).

The measured values of the nonlinear refractive index in crystals suggest that optical switching can be efficient. However, three-photon absorption at the wavelength used in experiments introduces certain limitations due to a decrease in the effective length of the nonlinear medium. The optical switching efficiency upon three-photon absorptions can be estimated from the critical condition

$$I < \frac{3\gamma}{\lambda \beta_{3\omega}}. \tag{13}$$

By substituting the measured values of the corresponding parameters into (13), we obtain the intensity $I = (4 - 7) \times 10^9$ W cm^{-2} below which BGO and BSO crystals can be used as optical switches at $\lambda = 1064$ nm.

3.2 Nonlinear crystal converters

The increase in the intensity of laser pulses due to the recent development of the techniques for generating and amplifying femtosecond laser pulses requires the consideration of the influence of higher-order optical processes on the second-order optical processes [42, 43]. Despite the fact that nonlinear crystal converters have been long used, their higher-order nonlinearities have been studied inadequately so far. The third-order nonlinear susceptibilities were measured only in some spectral regions and only for certain crystal orientations (see, for example, [11, 13, 44]). Therefore, analysis of the third-order nonlinear susceptibilities, nonlinear refractive indices, and nonlinear absorption coefficients of KDP, $LiNbO_3$, and BBO crystals at 1064 and 532 nm is of current interest.

The Kerr nonlinearities are estimated from an empirical model based on a simple assumption about a dominating influence of one efficient optical transition. The transition frequency λ_0^{-1} and the diagonal matrix element of the dipole moment operator μ_{01} are determined from the values of the refractive index and its dispersion. Unlike approximations [13, 45] used earlier, the values of the refractive index and its dispersion at the same transition frequency are used. In the single-transition approximation, the refractive index is determined by the known expression

$$n^2 = 1 + \frac{2}{c\hbar} \frac{f(\mu_{01}, \lambda_0, \lambda)\mu_{01}^2}{\lambda_0^{-1} - \lambda^{-1}} N. \tag{14}$$

Here, $f(\mu_{01}, \lambda_0, \lambda)$ is a factor taking into account the local-field correction and N is the density of oscillators. We can obtain from (14) the expression for the third-order nonlinear susceptibility responsible for the self-action, which has the form

$$\chi_K^{(3)} = \frac{1}{32\pi^3 c\hbar N} (n^2 - 1)\lambda^2 \frac{\partial n^2}{\partial \lambda}. \tag{15}$$

Expression (15) allows us to determine the dispersion of the Kerr nonlinearity from the refractive-index dispersion. In the general case the Kerr nonlinearity have tensor properties. Although the individual components of the

tensor of anisotropic crystals can be estimated from (15), the calculation of all components requires a more detailed analysis. A detailed analysis of the components of the nonlinear susceptibility tensor of a KDP crystal is presented in [46].

In the dispersionless approximation, the third-order Kerr nonlinearities of KDP crystals (the symmetry class $\bar{4}2m$) and $LiNbO_3$ and BBO crystals (the symmetry class $3m$) have four independent components. For the extraordinary wave directed at angles θ and φ to the crystal axes, the Kerr nonlinearity of a crystal of the symmetry $\bar{4}2m$ is expressed in terms of these components as

$$\chi_K^{(3)} = \frac{1}{4}\left[3(\chi_{1111} + \chi_{1122}) + (\chi_{1111} - \chi_{1122})\cos 4\varphi\right]\cos^4\theta + \frac{3}{2}\chi_{2233}\sin^2 2\theta + \chi_{3333}\sin^4\theta, \quad (16)$$

whereas the Kerr nonlinearity for a crystal of the symmetry $3m$ has the form

$$\chi_K^{(3)} = 3\chi_{1122}\cos^4\theta + 4\chi_{1123}(1 - 4\cos^2\varphi)\sin\varphi\sin\theta\cos^3\theta + \frac{3}{2}\chi_{2233}\sin^2 2\theta + \chi_{3333}\sin^4\theta. \quad (17)$$

It follows from (16) and (17) that the anisotropy of the Kerr nonlinearity is determined by the relation between its components and can be considerable. The consideration of the Kerr-nonlinearity dispersion increases the number of independent components up to five (the symmetry class $\bar{4}2m$) and six (the symmetry class $3m$).

The nonlinearities of some crystal converters measured by the z-scan method are presented in papers [46–48]. The experimental dependences of the normalised transmission of radiation through a limiting aperture on the sample position were interpreted by the method of the expansion of a Gaussian function, which is widely used to analyse the results of z-scan measurements [8], and by the numerical method in combination with the paraxial approximation [49, 50].

The physical foundation of the z-scan method is the inhomogeneous phase change in different regions of the beam with different radiation intensities. A change in the beam phase in nonlinear media can be caused, apart from self-action effects such as self-focusing and nonlinear absorption, by other parametric and combination processes. These processes are typical both for isotropic and anisotropic media. In anisotropic media with the high second-order nonlinearity, which is responsible for the second harmonic generation, a competing channel of the inhomogeneous change in the phase and intensity is the second harmonic generation and the inverse process [51] (second harmonic and subharmonic generation; this channel can be called conditionally the cascade channel).

In papers [46–48], nonlinear KDP, $LiNbO_3$ and BBO crystals of length from 0.8 to 2 cm cut at different angles to the optical axis were studied. Measurements were performed for different diffraction lengths R_d. The value of R_d was changed by mounting a telescope in front of a focusing lens. Table 2 presents the nonlinear susceptibilities and nonlinear refractive indices of these crystals calculated from the dependence of the normalised transmission of radiation at 1064 nm on z by using the processing method proposed in [8] and paraxial approximation [50].

The phase shift in BBO and $LiNbO_3$ crystals is positive, i.e. these crystals have self-focusing properties. Note that the phase shift in a $LiNbO_3$ crystal near $\theta = 90^\circ$ caused by the self-action channel only slightly exceeds the phase shift caused by the cascade process. The nonlinear absorption coefficient was estimated from open-aperture z-scan measurements. It was found that nonlinear absorption in this case was determined by the four-photon process. The four-photon absorption coefficient was measured to be 1.7×10^{-32} cm^5 W^{-3}. No nonlinear absorption was observed at 1064 nm in KDP and BBO crystals by the open-aperture z-scan method within the measurement sensitivity.

Table 3 presents the values of $\chi_K^{(3)}$, n_2, and γ measured at a wavelength of 532 nm. The diffraction length was the same and equal to $\sim$1 cm in all measurements. Measurements with KDP crystals were performed for the same orientation of the crystals and different intensities of the incident radiation. The nonlinearity of KDP crystals measured at 532 nm was smaller than that measured at 1064 nm. This agrees with calculations based on a simple empirical model.

Table 3. Nonlinear-optical parameters of crystal converters at 532 nm [48].

Crystal	L/cm	$\chi_K^{(3)}/10^{-14}$ cgs units	$n_2/10^{-13}$ cgs units	$\gamma/10^{-16}$ cm^2 W^{-1}
KDP ($\theta = 41^\circ$)	1.8	1.7	1.1	2.8
KDP ($\theta = 78^\circ$)	1.9	1.5	0.90	2.5
BBO ($\theta = 51^\circ$)	0.8	5.7	3.2	8.0

Table 2. Nonlinear-optical parameters of crystal converters at 1064 nm [48].

Crystal	L/cm	R_d/cm	Gaussian function-expansion approximation			Paraxial approximation		
			$\chi_K^{(3)}/10^{-14}$ cgs units	$n_2/10^{-13}$ cgs units	$\gamma/10^{-16}$ cm^2 W^{-1}	$\chi_K^{(3)}/10^{-14}$ cgs units	$n_2/10^{-13}$ cgs units	$\gamma/10^{-16}$ cm^2 W^{-1}
KDP ($\theta = 59^\circ$)	2	0.6	2.0	1.2	3.5	2.6	1.6	4.6
KDP ($\theta = 59^\circ$)	2	1.6	2.6	1.6	4.6	2.6	1.6	4.6
KDP ($\theta = 78^\circ$)	1.5	0.6	2.2	1.4	3.8	2.5	1.6	4.4
KDP ($\theta = 90^\circ$)	1.5	1.6	1.4	0.90	2.5	1.5	0.93	2.6
BBO ($\theta = 51^\circ$)	0.8	1.3	5.2	3.0	7.4	5.2	3.0	7.4
$LiNbO_3$ ($\theta = 90^\circ$)	0.8	1.3	6.9	2.9	5.4	7.5	3.2	6.0

The nonlinearity of the BBO crystal increased with decreasing wavelength, which also agrees with calculations taking into account the parameters of this crystal.

The dependence of the normalised transmission at 532 nm on the crystal position in limiting-aperture z-scan measurements exhibited asymmetry for all crystals, which is explained by the presence of nonlinear losses. Nonlinear absorption in KDP and BBO crystals is determined by three-photon processes, whereas nonlinear absorption in $LiNbO_3$ is determined by the two-photon process [47]. The three-photon absorption coefficients were 5.4×10^{-22} and 2.1×10^{-21} cm^3 W^{-2} for KDP and BBO crystals, respectively. The two-photon absorption coefficient measured for $LiNbO_3$ crystals (2.1×10^{-10} cm W^{-1}) was smaller than that calculated by expressions from [52] (2.9×10^{-9} cm W^{-1}), but better agrees with the value obtained in [53] (1.5×10^{-10} cm W^{-1}).

4. Fullerenes

Most of nonlinear-optical studies of fullerenes were performed earlier by the methods of degenerate four-photon mixing and third harmonic generation [54 – 59]. The nonlinear susceptibility $\chi^{(3)}$ of fullerenes in films and solutions responsible for phase conjugation at different wavelengths was investigated by the method of degenerate four-photon scattering [33, 60]. The nonlinear responses of similar fullerene systems responsible for the second- and third harmonic generation were studied in papers [61 – 65] and [61, 66, 67], respectively. It was found that C_{60} films have high third-order nonlinear susceptibilities at 1064 nm [$\chi^{(3)}(-3\omega;\omega,\omega,\omega) = 2 \times 10^{-10}$ cgs units and $\chi^{(3)}(-2\omega;\omega,\omega,0) = 2.1 \times 10^{-9}$ cgs units].

In fullerenes of interest is inverse saturated absorption, which determines an increase in absorption with increasing the laser radiation intensity [56, 68]. It is known that this effect is observed because the absorption cross section in excited states exceeds that from the ground state. Materials with inverse saturated absorption are excellent candidates for using them as optical limiters to protect eyes and other radiation detectors from intense laser pulses [69, 70].

The nonlinear-optical parameters of fullerenes C_{60} and C_{70} in polyamide films and toluene excited by 35-ps laser pulses at 1064 and 532 nm were analysed in papers [71 – 73]. The value of γ for the 0.5 % solution of C_{60} in toluene calculated from experimental data was -4×10^{-15} cm^2 W^{-1}. The nonlinear susceptibility of this sample was 2×10^{-13} cgs units at 1064 nm.

Measurements of the nonlinear absorption in samples showed that, within the accuracy of measurement of their transmission (2 %), this process was distinctly observed only in C_{60} solutions. Nonlinear absorption in this case could be caused by inverse saturated absorption due to excitation of fullerenes to higher-lying levels with absorption cross sections exceeding the ground-state absorption cross section. The nonlinear absorption coefficient of the 0.5 % solution of C_{60} in toluene was 1.5×10^{-10} cm W^{-1} at 1064 nm [71].

The inverse saturated absorption was observed in C_{60} and C_{70} films [58] and fullerene solutions [47, 68, 74] at the 532-nm second-harmonic wavelength of a Nd : YAG laser. The possibility of using fullerene-doped samples for optical limitation at 1064 nm was studied in [59]. The transmission in a cell with the 0.55 % C_{60} solution in toluene did not change with increasing the radiation intensity up to $I = 4 \times 10^{10}$ W cm^{-2}. Above this intensity, a decrease in transmission was observed. This effect was not observed in C_{70} solutions. Thus, it was shown in [59] that C_{60} solutions can limit the radiation intensity in the IR region as well.

Similar studies of the nonlinearity of fullerene-doped structures were also performed at a wavelength of 532 nm.

Table 4. Values and signs of $\mathrm{Re}\,\chi^{(3)}$ of the C_{60} solutions and films [72].

λ/nm	Sample	$\mathrm{Re}\,\chi^{(3)}$/cgs units	Experimental method	Pulse duration	References
532	C_{60}/toluene	-1.7×10^{-33}	SFWFM	25 ps	[54]
532	C_{60}/toluene	> 0	z-scan	19 ps	[56]
532	C_{60}/toluene	< 0	z-scan	70 ns [1)]	[56]
532	C_{60}/toluene	< 0 [2)]	z-scan	13 ps	[66]
532	C_{60}/toluene	$+5.8 \times 10^{-12}$	Ez-scan	15 ns	[57]
532	C_{60}/toluene	< 0	z-scan	30 ns	[55]
< 950	film C_{60} (5.2 μm)	< 0	z-scan	150 fs	[67]
532	C_{60}/toluene	> 0 [3)]	z-scan	23 ps	[68]
520	C_{60}/toluene	$-(3.4 \pm 0.7) \times 10^{-11}$ [4)]	z-scan	15 ns	[61]
576	C_{60}/ PMMA	< 0	shadow method	12 ns	[69]
532	C_{70}/liquid crystal	$+4.86 \times 10^{-8}$ cm^3 erg^{-1}	holographic recording	20 ns, 400 ps	[70]
532	C_{60}/metalloorganic solution	< 0 [5)]	z-scan	8 ns	[63]
532	C_{60}/metalloorganic solution	> 0 [6)]	z-scan	8 ns	[63]
532	C_{60}/toluene	$+(1.9 \pm 0.38) \times 10^{-13}$	z-scan	55 ps	[59]
532	film C_{60} (100 nm)	$+(4.8 \pm 0.96) \times 10^{-8}$	z-scan	55 ps	[59]

Notes: [1)] Pulse train of duration 19 ps (11 pulses in a train) with a pulse period of 7 ns; [2)] hyperpolarisability $\gamma' = \mathrm{Re}\,\chi^{(3)}/N = -4 \times 10^{-31}$ cgs units; [3)] $n_2 = 1.9 \times 10^{-12}$ cgs units; [4)] $\gamma = -(9.05 \pm 0.21) \times 10^{-13}$ cm^2 W^{-1}; [5)] $W = 20$ μJ; [6)] $W = 300$ μJ; SFWFM: stimulated four-wave frequency mixing.

Table 4 presents the values of $\mathrm{Re}\,\chi^{(3)}$ measured by different authors under similar spectral conditions. A great difference between the values of $\mathrm{Re}\,\chi^{(3)}$ and different signs of $\mathrm{Re}\,\chi^{(3)}$ can be caused by different experimental conditions (pulse duration, laser radiation intensity, etc.). In addition, the influence of nonlinearities of fullerene-doped matrices (toluene, polymers, and metallorganic compounds) can be also significant. A change in the radiation energy leads to a change in the sign of $\mathrm{Re}\,\chi^{(3)}$ for some fullerene-containing structures [51]. This can be caused by the influence of additional nonlinear-optical processes (thermal effect, Stark effect, etc.) proceeding along with the high-frequency Kerr effect.

The fifth-order nonlinearity of thin fullerene films was studied in [72]. It was shown that at low laser radiation intensities ($I_0 = 5 \times 10^8$ W cm^{-2}), the self-defocusing process is determined by third-order nonlinearities. The self-action type changed with increasing radiation intensity due to the increasing role of the higher-order (fifth) nonlinearity. Under these conditions, the self-defocusing properties of a thin (60 nm) fullerene film appeared. The nonlinear refractive indices caused by the third- and fifth-order processes at 532 nm were 2×10^{-9} cm^2 W^{-1} and -1.4×10^{-19} cm^4 W^{-2}, respectively.

In [73], the third harmonic generation (THG) was studied in fullerene-doped films. The nonlinear susceptibility of a polyamide film containing 0.5 % of C_{70} responsible for THG was 9×10^{-13} cgs units. The deviation of the dependence $I_{3\omega}(I_\omega)$ from a cubic dependence observed in experiments was explained by the influence of the Kerr nonlinearity on the phase relations between the pump and harmonic waves. The maximum THG conversion efficiency was 10^{-6}.

5. Dyes

5.1 Polymethine dyes

Practical applications of dyes in various problems of laser physics require the study of their optical parameters [75]. Along with common optical parameters, which have been already investigated to a great extent, an important characteristic of dyes is their nonlinear response to the action of short (picosecond and femtosecond) light pulses. It has been shown earlier that the nonlinear susceptibilities of a number of organic dye molecules with conjugated double bonds are comparable with the resonance nonlinear susceptibilities of atoms [76, 77]. Such molecules with double conjugated bonds and delocalised π electrons are very promising as nonlinear-optical media. Note that the delocalisation of π electrons in fullerenes is also responsible for the high nonlinear susceptibility of the latter [78, 79].

Mode locking devices based on polymethine dyes [80], which are used, as a rule, in problems of this type, are subjected to irreversible changes with time, which causes, in particular, variations in their nonlinear-optical parameters (for example, the saturation intensity and nonlinear absorption coefficient).

The nonlinear-optical parameters of polymethine dyes of different ionic characters: cationic (dyes 1–6), anionic (7), and neutral (8) were analysed in paper [81] by the z-scan method in the field of picosecond pulses. The numeration of dyes corresponds to the classification presented in [80]. The z-scan experiments were performed by using a picosecond 1064-nm Nd : YAG laser emitting 55-ps, 2-mJ pulses with a pulse repetition rate of 2 Hz. The dye solutions were z-scanned by using the open-aperture scheme. The value of β for the solution of dye 2 (at the concentration $C = 2.5 \times 10^{-3}$ M) was measured to be 3×10^{-13} cm W^{-1}. Note that calculations performed earlier showed that some of the dyes (tetracene, paraterphenyl, pentacene) have considerable Kerr nonlinearities [82].

Similar measurements were performed for all other dyes. Their nonlinear refractive indices are presented in Table 5, where are also given coefficients β measured for these dyes at different concentrations. One can see that, having rather low nonlinear refractive indices (at the given concentrations of solutions), some of the dyes exhibit noticeable nonlinear absorption. This can be explained both by inverse saturated absorption and two-photon absorption. It was found that, unlike other dyes, no nonlinear-optical effects were observed for dye 7 (the data for dye 7 are not presented in Table 5).

Table 5. Nonlinear-optical parameters of polymethine dyes [81].

Dye number	$C/10^{-3}$ M	$\gamma/10^{-16}$ cm^2 W^{-1}	$\beta/10^{-13}$ cm W^{-1}	I_s/ W cm^{-2}
1	2.8	2.6	2.3	–
2	2.5	5.6	3.0	–
3	2	4.5	1.7	–
4	2	–	–	4×10^8
5	1.3	–	–	3.4×10^6
6	1.6	65	–	–
8	4.5	2.7	–	–

Dye 5 is of certain interest among polymethine dyes. This dye is also known as dye 269u. Due to efficient lasing of this dye in polyurethane matrices and alcohol solutions observed in a broad range of 80 nm at 1150 nm upon pumping at 1064 nm [83], the dye is promising not only as a saturable absorber for passive mode locking but also as a laser medium for generating ultrashort IR pulses due to a large width of its lasing spectrum.

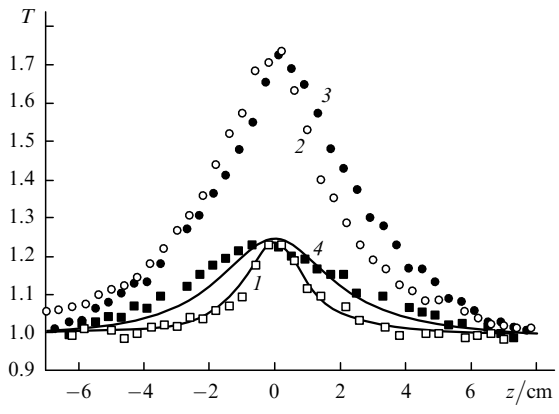

Figure 6. Dependences of the normalised transmission of the dye 5 solution on z in the open-aperture scheme for radiation intensities in the focal plane 1.2×10^7 (*1*), 4.8×10^7 (*2*), 1.5×10^8 (*3*), and 1.2×10^9 W cm^{-2} (*4*). The solid curves are theoretical calculations for the minimal (*1*) and maximal (*4*) laser radiation intensities [81], circles and squares are experiment.

The results of the open-aperture z-scan measurement of saturated absorption in dye 5 in ethanol at different radiation intensities are presented in Fig. 6 in the form of the dependences of the normalised transmission of the dye 5 solution on z. At low laser radiation intensities, the normalised transmission increases with increasing radiation intensity, which is typical for saturable absorbers. As the radiation intensity was further increased, absorption was saturated, the envelope of the dependence $T(z)$ broadened, and then nonlinear absorption appeared, which was caused by either multiphoton absorption or inverse saturated absorption and manifested in a decrease in the maximum value of the normalised transmission. These dependences can be used to determine the intensity regions where the conditions of the maximum bleaching of the dye are fulfilled and at the same time the influence of other nonlinear-optical processes, in particular, nonlinear absorption is absent.

In the trivial case of a linear dependence of the absorption coefficient α on the radiation intensity, this coefficient can be described by expression (11), where the linear absorption coefficient can be, in particular, negative in the case of saturated absorption.

There also exist other models describing saturated absorption. For a two-level system with the inhomogeneous broadening, the equation describing the saturation process can be written in the form [84]

$$\alpha = \alpha_0 \frac{1}{(1 + I/I_s)^{0.5}}. \tag{18}$$

Here, I and I_s are the laser radiation and saturation intensities, respectively. Another ('kinetic') model is used in the case of the depletion of the ground-state concentration and gives the relation [85]

$$\alpha = \alpha_0 \frac{1}{1 + I/I_s}. \tag{19}$$

Yet another ('three-level') model giving the expression

$$\alpha = \alpha_0 \frac{1}{1 + (I/I_s)^{0.5}} \tag{20}$$

was used in [86] to analyse saturated absorption.

The experimental dependence of the saturated absorption in the dye 5 solution is well described by the three-level model at low radiation intensities and by the two-level model with the inhomogeneous broadening at high radiation intensities.

5.2 Organic dye vapours

The nonlinear-optical properties of vapours of organic molecules were first studied in the benzene C_6H_6 vapour [87], where radiation was converted to the vacuum UV region, and also in the acetylene C_2H_2 vapour, where THG in the UV region was performed in a dye laser [88]. The nonlinear-optical parameters of organic dye vapours were studied in papers [89, 90], where various schemes for radiation frequency conversion were proposed.

The frequency conversion of picosecond IR pulses and UV radiation upon THG in organic dye vapours were analysed in paper [91]. The dipole moments and nonlinear susceptibilities of organic dye vapours were calculated by using the free electron model. Although this model is simplified [92], it allows one to calculate quite accurately the optical and nonlinear-optical spectral parameters of systems with conjugated double bonds [93].

The THG of laser radiation in organic dye vapours was studied by the example of naphthalene $C_{10}H_8$. Note that naphthalene was chosen because its vapour has a high enough concentration already at relatively low temperatures ($\sim$200 °C), which is required to achieve the synchronous interaction between the pump and harmonic waves. By using the energy levels, frequencies, and transition dipole moments calculated for naphthalene and relations presented in [93], the third-order nonlinear susceptibility $\chi^{(3)}(3\omega)$ was calculated for a single molecule to be 0.42×10^{-34} cgs units (for the THG of the Nd:YAG laser radiation, $\omega + \omega + \omega = 3\omega$).

Third harmonic generation in isotropic media can be performed not only in the scheme $\omega + \omega + \omega = 3\omega$, but also in the scheme $\omega + \omega - \omega = 3\omega$. The fifth-order nonlinear susceptibility $\chi^{(5)}(3\omega)$ calculated according to the latter scheme is 1.3×10^{-46} cgs units.

In [91], a Nd:YAG laser emitting trains of picosecond pulses was used as a radiation source. The pulse duration was 35 ps and the energy of the pulse train was 5 mJ. Laser radiation was focused by a lens with a focal distance of 25 cm to the centre of a cell with naphthalene vapour. The cell was heated up to 220 °C to obtain the naphthalene concentration of $\sim 10^{18}$ cm^{-3}. The pump and third harmonic radiation at 354.7 nm was coupled out through the output quartz window and directed to a spectrograph.

Figure 7 shows the dependence of the third-harmonic intensity on the naphthalene vapour temperature. The maximum intensity of converted radiation was achieved at 170 °C. The maximum THG efficiency in naphthalene vapour was 10^{-8}. Such a dependence is typical for generation of odd harmonics upon tight focusing ($b \ll L$, where $b = 8$ mm is the confocal diameter of focused radiation, and $L = 180$ mm is the length of the nonlinear medium) in an isotropic nonlinear medium with the anomalous dispersion and also for generation of the difference frequency by neglecting the sign of the medium dispersion.

As mentioned above, THG in naphthalene vapour can occur through two channels: the direct four-photon ($\omega + \omega + \omega = 3\omega$) and six-photon generation of the difference frequency ($\omega + \omega + \omega + \omega - \omega = 3\omega$). The necessary condition for synchronous THG to proceed through the first channel upon tight focusing of the incident radiation to the nonlinear medium is the falling of the third harmonic

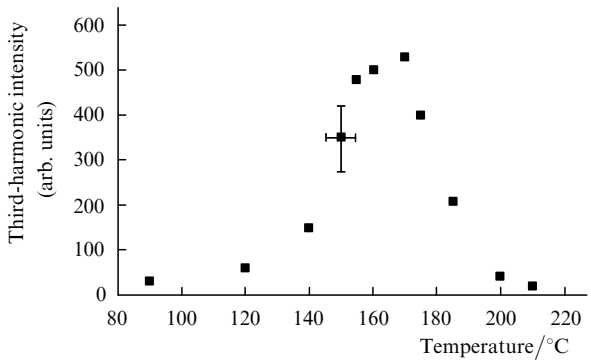

Figure 7. Dependence of the third-harmonic intensity of the naphthalene vapour temperature [91].

wavelength to the anomalous dispersion region (i.e. the condition $k_3 - 3k_1 < 0$ should be fulfilled, where k_3 and k_1 are the wave numbers of the harmonic and pump radiation, respectively). Only in this case, the additional phase shift appearing after the propagation of radiation through the focal region is compensated by the dispersion of the nonlinear medium, which provides conditions for the synchronous interaction of the pump and harmonic waves. Analysis of one-photon absorption in naphthalene vapour shows that no absorption bands are observed near the third harmonic wavelength (354.7 nm) [94]. Naphthalene has the normal dispersion in this spectral range. For this reason, the condition of synchronous interaction of the waves in the channel $\omega + \omega + \omega = 3\omega$ for naphthalene vapour is not fulfilled for moderate output powers of the Nd : YAG laser, when the influence of the optical Kerr effect is not sufficient for changing the sign of dispersion.

For THG via the second channel, the situation is different. The presence of the negative dispersion region is no longer required for the $\omega + \omega + \omega + \omega - \omega = 3\omega$ process to occur, because the difference frequency can be generated in the synchronous regime in media with different signs of dispersion [16, 95]. Therefore, in this case, the most probable is the fifth-order process. The nonlinear susceptibility $\chi^{(5)}$ of this process, as $\chi^{(3)}$, will be determined by the presence of lines with large oscillator strengths near the four-photon resonance. A similar process of the difference-frequency generation in naphthalene vapour at the second-harmonic wavelength of a Nd : YAG laser was studied earlier upon four-photon interaction ($2\omega + 2\omega - \omega = 3\omega$) [90].

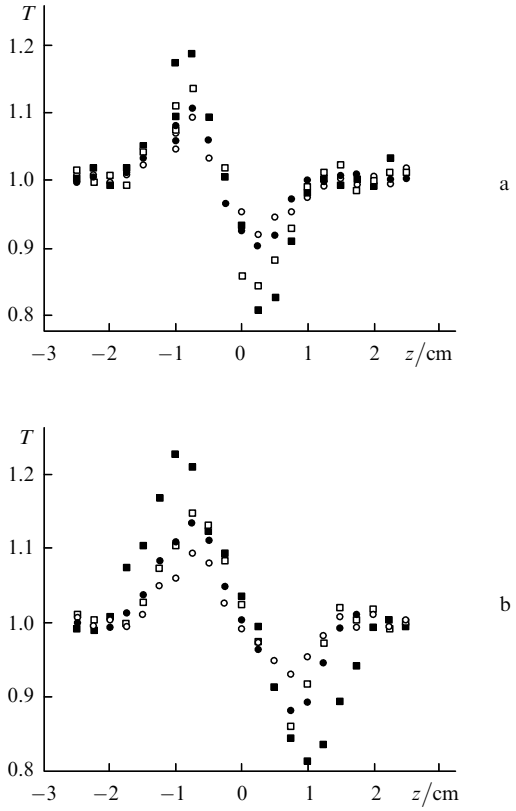

Figure 8. Dependences of the normalised transmission of PVP solutions with the cobalt concentration 2 % (○), 5.3 %(●), 6.2 % (□), and 13.5 % (■) [98] in the limiting-aperture scheme at 1064 (a) and 532 nm (b).

6. Metals

6.1 Organometallic structures

Doping metals into polymer structures changes both optical and nonlinear-optical parameters of these composite materials [96, 97]. In [96], complexes of polymers with metals were studied with the aim of using them for optical switching and optical limitation in the field of nanosecond pulses. In [97], porphyrin polymers doped with zinc were investigated for the purpose of using them for optical limitation. It was shown that these compounds can efficiently limit the intensity of 500-ps laser pulses at a wavelength of 532 nm. Note that optical limitation in polymer metal-containing complexes was mainly studied in the visible spectral region.

In [98], the nonlinear-optical parameters of polyvinyl pyrrolidone (PVP) doped with various metals were investigated. An attractive feature of PVP is that this polymer does not lose its good optical properties (in particular, weak scattering of light) upon doping with molecules and atoms. Note that PVP can be also used as a stabilising reagent for such nanostructures as metal clusters, which makes it attractive for the development of stable suspensions used in nonlinear-optical studies [99].

The aqueous solutions of PVP doped with cobalt at different concentrations (2 %, 5.3 %, 6.2 %, and 13.5 %) and with iron (4.25 %) and zinc (0.85 %) were investigated. One gram of a metalllopolymer was dissolved in 100 ml of distilled water at room temperature. Solutions were studied in cells of thickness 1 mm (in z-scan experiments) and 2 mm (in THG experiments). Figure 8a presents the normalised transmissions of organometallic polymers at 1064 nm with different cobalt concentrations as functions of z. Figure 8b presents similar dependences obtained at 532 nm. Note that the nonlinearity sign is constant in the case of these two wavelengths. One can see from Fig. 8 that transmission increases with increasing cobalt concentration. This is explained by the enhancement of defocusing with increasing Co concentration. Experiments with pure water and pure PVP (without cobalt) did not reveal the characteristic nonlinear dependence of $T(z)$.

The open-aperture z-scan studies showed that nonlinear absorption at 532 nm was observed for all samples. The nonlinear absorption coefficient of the PVP solution with cobalt at a concentration of 13.5 % was 9.4×10^{-10} cm W^{-1}. Nonlinear absorption at 1064 nm was not observed, although high-power radiation was used. A decrease in transmission at 532 nm was caused by inverse saturated absorption, which is manifested in many similar organometallic and polymer structures in the visible spectral range [100 – 102]. In [101], nonlinear absorption in metalloporphyrins was studied. It was shown that nonlinear absorption at 532 and 600 nm (in the field of picosecond and nanosecond pulses) was caused by inverse saturated absorption. The absence of nonlinear, in particular, two-photon absorption at 1064 nm is probably explained by the fact that the resonance line of metalloporphyrin solutions lies outside the region of the two-photon transition at this wavelength.

Table 6 presents the nonlinear refractive indices, Kerr nonlinear susceptibilities, and nonlinear absorption coefficients of organometallic polymers measured in [98].

Table 6. Nonlinear refractive indices, nonlinear absorption coefficients, and nonlinear susceptibilities of Co solutions in PVP [98].

Substance	λ/nm	$\gamma/10^{-15}$ cm^2 W^{-1}	$\beta/10^{-10}$ cm W^{-1}	$\chi^{(3)}/10^{-14}$ cgs units
PVP (2 % Co)	1064	−0.9	–	−6.87
PVP (5.3 % Co)	1064	−1.4	–	−11
PVP (6.2 % Co)	1064	−1.8	–	−13.8
PVP (13.5 % Co)	1064	−2.6	–	−19.7
PVP (2 % Co)	532	−1.6	2.1	−11.8
PVP (5.3 % Co)	532	−3.4	4.2	−26.5
PVP (6.2 % Co)	532	−4.6	6.1	−35.9
PVP (13.5 % Co)	532	−6	9.4	−47

One of the mechanisms providing highly efficient nonlinear absorption is, as mentioned above, the inverse saturated absorption. Absorption of this type was successfully described by the so-called five-level model [103]. The inverse saturated absorption can be observed if a medium satisfies the following criteria. First, the excited-state absorption cross section of the medium should exceed the ground-state absorption cross section. Second, the excited-state lifetime should be long enough compared to the exciting pulse duration. A number of organometallic materials found recently such as metalloporphyrins [101, 104], metallopolyenes [105], and metallophthalocyanines [100] satisfy these criteria. It was quite reasonable to expect the presence of inverse saturated absorption in structures that we studied (along with other possible optical limitation mechanisms).

In [106], the optical limitation process was studied in PVP metal complexes at 1064 and 532 nm. Despite the absence of nonlinear absorption in the IR region, the PVP metal complexes, as shown above, exhibit distinct defocusing properties. This circumstance suggested the possibility of using self-action (in this case, self-defocusing) to obtain optical limitation in the IR region.

Figure 9 presents the dependences of the normalised transmission of PVP solutions with different cobalt concentrations on the incident radiation intensity at 1064 nm obtained by the limiting-aperture z-scan method. In this case, cells with solutions were located in the region of minimal transmission, i.e. in the region of the dip in the dependence $T(z)$ (Fig. 8).

A different situation was observed for $\lambda = 532$ nm (Fig. 9). In this case, optical limitation was caused both by self-defocusing (playing a decisive role for IR radiation) and by nonlinear absorption (to a greater extent). Nonlinear absorption could be caused by two-photon absorption and inverse saturated absorption (at high radiation intensities). However, the contributions of these processes cannot be estimated due to the absence of data on the spectral parameters and lifetimes of the excited singlet and triplet states of metal complexes studied in these experiments.

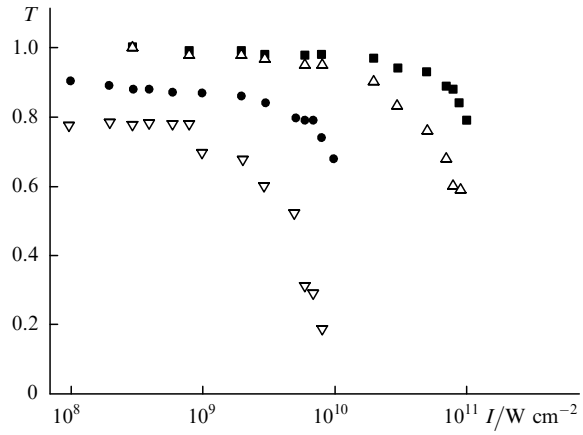

Figure 9. Normalised transmission as a function of the radiation intensity at wavelengths 1064 (■,△) and 532 nm (●,▽) for the cobalt concentration in PVP equal to 2 % (■,●) and 13.5 % (△,▽) [106].

Theoretical curves constructed taking into account only two-photon absorption differ somewhat from experimental data (Fig. 9). The experimental curves demonstrate the gently sloping optical limitation unlike theoretical estimates. This is explained by the additional influence of inverse saturated absorption and self-defocusing.

The nonlinear-optical parameters of PVP solutions doped with iron and zinc were studied in [107] by using 35-ps, 1-mJ third-harmonic pulses from a picosecond 1064-nm Nd : YAG laser. The laser radiation was focused by a lens with a focal distance of 25 cm into quartz cells with solutions of metallopolymers. The 354.7-nm third-harmonic radiation was filtered from the pump radiation and directed to a diffraction spectrograph. The aqueous solutions of PVP doped with iron (4.25 %) and zinc (0.85 %) were studied.

Figure 10 shows the dependence of the third-harmonic intensity on the pump radiation intensity for the PVP solution with iron (Fe : PVP). The slope of the dependence $I_{3\omega}(I_0)$ was 2.85 over the entire interval of intensities, which is close to the expected result. A similar dependence was also obtained for the PVP solution with zinc (Zn : PVP). The maximum pump-conversion efficiencies for PVP solutions doped with zinc and iron were 8×10^{-7} and 5×10^{-7}, respectively.

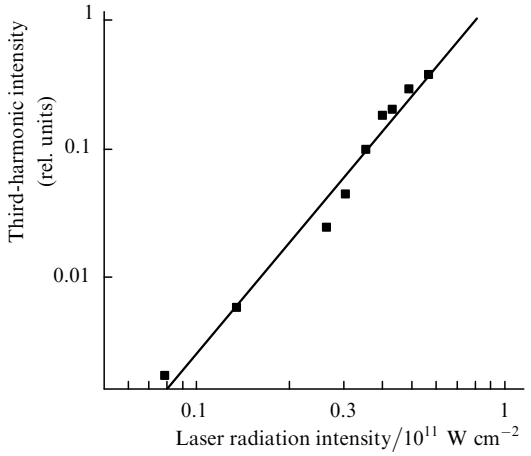

Figure 10. Dependence of the third-harmonic intensity on the laser radiation intensity for Fe : PVP [107].

The nonlinear susceptibility responsible for THG is determined by the expression [108]

$$\left|\chi^{(3)}\right|^2 = \frac{\lambda_1^2 n_3 n_1^3 c^2 \eta}{256\sqrt{3}(\ln^3 2)\pi^5 L^2 I_\omega^2}\left[\frac{\sin(\Delta kL/2)}{\Delta kL/2}\right]^{-2}, \qquad (21)$$

where λ_1 and I_ω are the wavelength and intensity of the fundamental radiation; n_1 and n_3 are the refractive indices of the medium at the pump and harmonic wavelengths, respectively; η is the conversion efficiency; $\Delta k = 6\pi(n_3 - n_1)/\lambda_1$ is the difference of wave numbers of the harmonic and pump, respectively. The nonlinear susceptibilities of Zn : PVP and Fe : PVP, calculated from (21), were 5×10^{-13} and 3×10^{-13} cgs units, respectively.

6.2 Colloidal metal solutions

Colloidal metal solutions have high nonlinear-optical coefficients and a fast response [109, 110], especially in the frequency range of their surface plasmon resonances. Most of the nonlinear-optical studies of colloidal metal solutions have been performed by the method of four-photon mixing. It was shown already in the first experiments on phase conjugation in colloidal gold and silver [111] that the reflection coefficient of the conjugate wave considerably increased near the plasmon-resonance surface. A number of promising colloidal metal solutions were found for applications in optical limiters.

The authors of paper [112] determined the relation between associates of small particles in hydrosols of noble metals and the presence of fractal properties of the latter. It was shown in [110, 113] that colloidal copper solutions have a high nonlinear refractive index. Similar results were obtained for silver [109, 114] and gold [115, 116] solutions. The nonlinear susceptibility of silver and gold hydrosols was investigated in [109, 115]. It was shown that the susceptibility varied from 10^{-11} to 10^{-13} cgs units for colloidal gold depending on the volume fraction of metal particles in the solvent. At the same time, the nonlinear susceptibilities of metal silver and gold particles themselves were $(1-5) \times 10^{-8}$ and $(2-4) \times 10^{-9}$ cgs units, respectively.

In [116], the nonlinear-optical parameters of colloidal solutions of some metals (silver, gold, copper, and platinum) prepared by the chemical method were studied. The absorption spectra of these solutions changed after irradiation by picosecond laser pulses. The absorption spectrum of gold had the maximum at 525 nm before irradiation, in accordance with data published earlier [117]. However, the frequency of the surface plasmon resonance (SPR) of gold nanoparticles shifted to the red (525–550 nm) after irradiation at 1064 nm. This shift was caused by the aggregation of gold particles induced by irradiation. A similar picture was also observed in aqueous solutions of some other metals, in particular, silver.

Colloidal silver particles are classical objects for studying optical phenomena in ultradispersion metal systems. The surface plasmon resonance of silver hydrosols (410–420 nm) [118] determines the shape of their optical spectra. Aggregation induced by irradiation, which was earlier observed in colloidal silver solutions [119], resulted both in the SRP frequency shift and corresponding variations in some nonlinear-optical parameters. The appearance of the long-wavelength wing in the absorption spectrum of the silver hydrosol was explained in [116] by the aggregation of silver particles to fractal clusters, accompanied by the frequency shift of the intrinsic optical resonances of particles due to dipole–dipole interaction of the photoinduced dipole moments of each particle with the dipole moments of nearest-neighbour particles.

The photoinduced formation of aggregates in colloidal metal systems have been studied in many papers [118, 120], where changes in the size of aggregates were judged from changes in the absorption spectrum. A drastic increase in the photoinduced aggregation rate has been observed in a number of papers [118, 119]. In the present paper, we assume that aggregation is caused by photoeffect inducing the formation of oppositely charged particles due to the mutual exchange by photoinduced electric charges between particles of different sizes via a conducting medium. It was found in [116] that the nonlinear refractive index at 1064 nm was positive for all colloidal solutions studied except the gold solution. This picture was also preserved for all solutions irradiated by the second harmonic of a Nd : YAG laser at 532 nm except the copper solution, in which the sign of γ changed. Analysis of nonlinear absorption in these solutions showed that this process was distinctly observed only for colloidal gold. Nonlinear absorption in this case could be caused by inverse saturated absorption due to excitation of aggregates to higher-lying levels with larger absorption cross sections compared to the ground-state absorption cross section.

6.3 Solid dielectric matrices doped with metals

Composite materials based on solid dielectric matrices doped with metal nanoparticles attracted interest more than two decades ago [121]. The study of these materials still attracts great attention [122–125] because they are promising for applications in fast optical switching systems and optical limiters. In [126–129], the nonlinear-optical properties of copper and silver nanoparticles in glass matrices were studied in the UV, visible, and IR spectral regions. Silica glasses (SG) containing 100 % of SiO_2 and the SLSG silica glass containing 70 % of SiO_2, 20 % of Na_2O and 10 % of CaO were used. These glasses were irradiated by the 60-keV Ag^+ и Cu^+ beams with doses 4×10^{16} and 8×10^{16} ion cm^{-2}. The penetration depth of metal nanoparticles was 60 nm. The average size of Cu nanoparticles measured by the method of X-ray reflectometry was 3–5 nm. The size of silver nanoparticles varied in a broader range (from 2 to 18 nm). The formation of metal nanoparticles was also confirmed by the appearance of characteristic absorption lines in the ranges from 400 to 450 nm (for silver-doped glasses) and 550–600 nm (for copper-doped glasses) corresponding to the SPR frequencies of silver and copper nanoparticles.

The nonlinearity of samples in different spectral regions was studied in [126–129] by using radiation of a picosecond Nd : YAG laser and its second and third harmonics. The 1064-nm Nd:YAG laser emitted 55-ps, 1-mJ pulses with a pulse repetition rate of 2 Hz. In Cu : SG and Cu : SLSG samples, self-defocusing and self-focusing was observed, respectively, thereby demonstrating the important role of a matrix in the proceeding of a nonlinear-optical process. The values of β for SLSG and Cu :zSLSG were 2.3×10^{-16} and 1×10^{-10} cm^2 W^{-1}, respectively. The values of β for Cu : SLSG and Cu : SG ($\lambda = 1064$ nm) were 3.4×10^{-6} and 9×10^{-6} cm W^{-1}, respectively. The nonlinear susceptibility of Cu : SG was 2.4×10^{-8} cgs units [126].

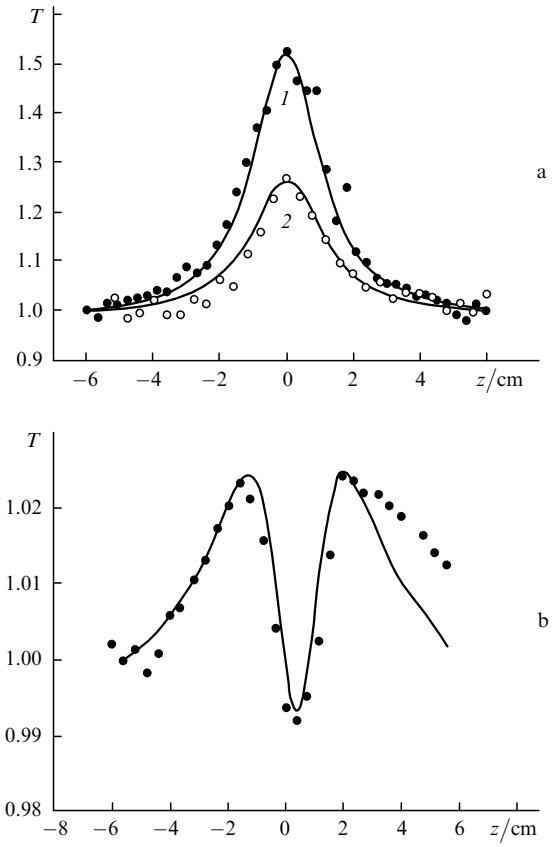

Figure 11. Dependences of the normalised transmission of Ag : SLSG (*1*) and Ag : SG (*2*) (a) and Cu : SG (b) on z in the open-apertures scheme at 532 nm. The solid curves are theoretical calculations [127], circles are experiment.

Self-focusing at 1064 nm was observed for both samples containing silver. As in the case of copper nanoparticles, the SPR frequency of compounds containing silver nanoparticles depended on the matrix. Surface plasmon resonances in Ag : SG and Ag : SLSG were located in the regions of 415 and 440 nm, respectively.

Figure 11a shows the dependences of the normalised transmission of Ag : SG and Ag : SLSG obtained by the open-apertures z-scan method by irradiating samples at 532 nm with intensity 2.5×10^9 W cm^{-2}. The transmission of samples increased with increasing laser radiation intensity due to saturated absorption. The agreement between theoretical and experimental curves was achieved for the nonlinear absorption coefficients of Ag : SLSG and Ag : SG equal to -6.7×10^{-5} and -3.6×10^{-5} cm W^{-1}.

The dependence of the normalised transmission of Cu : SG on z in this spectral region (Fig. 11b) can be determined by competition between saturated absorption and inverse saturated absorption. In this case, the nonlinear absorption coefficient responsible for the latter process was equal to 6×10^{-6} cm W^{-1}. It was found in [128] that nonlinear refractive indices and the real parts of the nonlinear susceptibilities of samples containing silver nanoparticles were -4.1×10^{-10} cm^2 W^{-1} and -2.4×10^{-8} cgs units at 532 nm, respectively, for Ag : SLSG and -6.2×10^{-10} cm^2 W^{-1} and -3.5×10^{-8} cgs units, respectively, for Ag : SG.

Nonlinear-optical studies of metal nanoparticles were earlier performed, as a rule, in the visible and near-IR regions. However, these structures can have interesting nonlinear-optical properties in the UV region [128]. In [129], silver and copper nanoparticles doped into various glass matrices were studied upon irradiation by 55-ps, 0.1-mJ, 354.7-nm third-harmonic pulses from a Nd : YAG laser. The dependence of the normalised transmission on z obtained by the limiting-aperture z-scan method showed that Ag : SG has the negative values of the nonlinear refractive index and saturated absorption ($\gamma = -7.6 \times 10^{-10}$ cm^2 W^{-1} and $\beta = -1.4 \times 10^{-5}$ cm W^{-1}). Similar measurements for Cu : SG samples gave $\gamma = -1.7 \times 10^{-10}$ cm^2 W^{-1} and $\beta = -6.7 \times 10^{-6}$ cm W^{-1}.

7. Semiconductors

7.1 Chalcogenide films

The large nonlinearity, high transparency in the IR region and the possibility of simple processing of chalcogenide structures stimulated extensive investigations on nonlinear refraction and nonlinear absorption in these structures [130 – 132]. The nonlinear refractive indices and nonlinear absorption coefficients of a number of chalcogenide glasses have been studied in [133, 134]. The nonlinear parameters of these glasses strongly depend on the wavelength. Thus, the nonlinear refractive index and nonlinear absorption coefficient of As_2S_3 at 633 nm are 7.6×10^{-5} cm^2 W^{-1} and 1.6 cm W^{-1}, respectively [135], whereas these quantities in the IR region are 5.7×10^{-14} cm^2 W^{-1} and 2.6×10^{-10} cm W^{-1}, respectively [136] (at 1064 nm) and 1.7×10^{-14} cm W^{-1} [137] (at 1319 nm).

Recently, thin chalcogenide films have attracted great attention. The parameters of these films depend both on the growth conditions and external factors. The influence of irradiation on the optical properties of thin amorphous AS_2S_3 films has been studied in [138].

The influence of nonlinear refraction and nonlinear absorption in a number of chalcogenide films on the optical limitation of the intensity of picosecond laser pulses was studied in [139]. Chalcogenide films As_2S_3, $As_{20}S_{80}$, $2As_2S_3/As_2Se_3$, and $3As_2S_3/As_2Se_3$ were investigated. The films were deposited on the surface of BK-7 glass plates by vacuum evaporation of the crushed components of chalcogenide glasses (As_2S_3, $As_{20}S_{80}$, As_2Se_3). Amorphous multilayer films $2As_2S_3/As_2Se_3$ and $3As_2S_3/As_2Se_3$ were prepared by evaporating by turn As_2S_3 and As_2Se_3. The ratio of thicknesses of film monolayers was 20 nm : 10 nm (for $2As_2S_3/As_2Se_3$) and 30 nm : 10 nm (for $3As_2S_3/As_2Se_3$). The thickness of all the films was 10 μm. The films were irradiated by 1064-nm picosecond pulses from a Nd : YAG laser and its second harmonic at 532 nm.

The z-scan studies showed that the nonlinear refractive index of the $2As_2S_3/As_2Se_3$ and $3As_2S_3/As_2Se_3$ films is negative, resulting in self-defocusing in these films, whereas this parameter for chalcogenide As_2S_3 and $As_{20}S_{80}$ films is positive and self-focusing occurs in them. The third-order nonlinearity at low laser radiation intensities was caused by nonlinear refraction related to bound electrons [140]. At high radiation intensities, the influence of nonlinear refraction caused by free carriers generated upon two-photon absorption becomes noticeable. The authors of paper [141] assumed the influence of the fifth-order nonlinearity corresponding to the negative nonlinear addition to the refractive index. For this reason, the nonlinear refractive index was

determined in [139] by using laser radiation intensities at which the influence of nonlinear absorption was insignificant. In particular, the value of γ was determined by using the intensity $I = 2 \times 10^8$ W cm^{-2} at which a change in the refractive index was caused only by the third-order nonlinearity. The absence of the influence of free charge carriers on the change in the refractive index was indirectly confirmed by the symmetric dependence $T(z)$ in the limiting-aperture scheme (for all films, except $As_{20}S_{80}$).

It was shown in [139] that the value of γ for some chalcogenide films is quite large. Thus, the nonlinear refractive index of an $As_{20}S_{80}$ film was 5×10^{-11} cm^2 W^{-1} at 532 nm. The greatest value of γ equal to -1×10^{-10} cm^2 W^{-1} at 1064 nm was observed for a $2As_2S_3/As_2Se_3$ film. Two-photon absorption was observed in all semiconductor structures studied. The values of β measured for chalcogenide films $As_{20}S_{80}$ ($\beta = 3 \times 10^{-6}$ cm W^{-1} at 532 nm) and $3As_2S_3/As_2Se_3$ ($\beta = 10^{-7}$ cm W^{-1} at 1064 nm) show that thin chalcogenide films have also large nonlinear absorption coefficients.

It was found that the nonlinear refractive index of As_2S_3 films for radiation intensities used in experiments has the same sign as for bulk structures (as expected). This also corresponds to the model based on the Kramers–Kronig relations, which predicts that semiconductors for which the relation $\hbar\omega/E_g < 0.69$ is fulfilled should have the positive nonlinear refractive index [142]. Here, E_g is the energy gap width. The value of E_g for As_2S_3 is 2.37 eV, and the corresponding value of $\hbar\omega/E_g$ at 1064 nm is 0.49.

A different situation was observed for an $As_{20}Se_{80}$ film. The value of E_g for this film is 2.5 eV. The parameter $\hbar\omega/E_g$ at 532 nm in this case is 0.93, and therefore the film should have self-defocusing properties. However, experiments showed that the value of γ for this film is positive.

A similar situation was also observed for multilayer films $2As_2S_3/As_2Se_3$ and $3As_2S_3/As_2Se_3$. The calculated energy gap widths of multicomponent films $2As_2S_8/As_2Se_3$ and $3As_2S_8/As_2Se_3$ (taking into account the extrapolation of data [143]) were 1.97 and 1.99 eV. Having these values of E_g and the corresponding values of the parameter $\hbar\omega/E_g$ equal to 0.59 for $2As_2S_3/As_2Se_3$ and 0.58 for $3As_2S_3/As_2Se_3$, these films should have self-focusing properties ($\gamma > 0$) at 1064 nm. However, experiments showed that $2As_2S_3/As_2Se_3$ и $3As_2S_3/As_2Se_3$ films exhibit self-defocusing.

The reason for such behaviour is not clear. It was assumed in [139] that free carriers affected the general picture of phase relations for radiation propagating through the film (due to two-photon absorption, this influence, although weak, could be manifested at radiation intensities used in experiments). It is known that a change in the refractive index is determined in the general case by the relation

$$\Delta n = \gamma I + \sigma_r N. \qquad (22)$$

Here, the second term of the sum is the additional change in the refractive index caused by the influence of free charge carriers. The parameter σ_r characterises a change in the refractive index caused by a single free charge carrier formed in various processes of photoexcitation and ionisation, which produce the cloud of charge carriers of density N. The parameter σ_r for most of the semiconductors is negative and can compensate and even exceed the positive addition to the refractive index due to the influence of bound electrons. The latter circumstance can change the behaviour of laser radiation propagating through the medium (from self-focusing to self-defocusing). Another possible reason for the observed picture can be interference in thin films resulting in the increase in the local-filed factor, two-photon absorption, and the influence of free charge carriers on the refractive index of the medium.

Optical limitation in semiconductors was studied by the open-aperture z-scan method. Figure 12 presents the dependences of the transmission of a number of films on the laser radiation intensity. The sample position corresponded to the transmission minimum, i.e. it was located at the focal point. Optical limitation in this case was caused by two-photon absorption. The strongest limitation (by 25 times) was observed in As_2S_3.

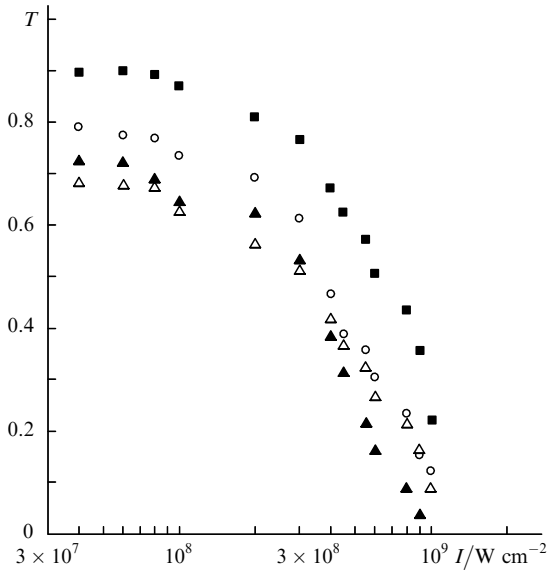

Figure 12. Dependences of the normalised transmission of chalcogenide films $As_{20}S_{80}$ (■), $2As_2S_3/As_2Se_3$ (○), As_2S_3 (▲), and $3As_2S_3/As_2Se_3$ (△) on the incident radiation intensity at 1064 (○, ▲, △) and 532 nm (■) in the open-aperture scheme.

7.2 Colloidal semiconductor solutions

Colloidal solutions are often prepared by chemical methods [144, 145]. Laser ablation (i.e. sputtering of an initial material by a focused laser radiation) can be also efficiently used to prepare various colloidal solutions of nonlinear-optical materials [146]. Laser ablation has been mainly applied to noble metals. At the same time, the extension of a scope of promising materials is of certain interest. Semiconductor structures can be one of such materials [147].

The aqueous colloidal solutions of the As_2S_3 and CdS semiconductors obtained by the laser ablation method were studied in [148, 149]. The colloidal solutions of semiconductor nanoparticles were prepared by using a Q-switched 1064-nm Nd : YAG laser emitting 20-ns, 15-mJ pulses at a pulse repetition rate of 10 Hz. Samples (As_2S_3 chalcogenide glass or crystalline CdS) were placed into a 5-cm-thick quartz cell filled with distilled water or organic solvents (xylene, toluene, ethanol). The laser radiation was focused by a lens with a focal distance of 8 cm on the surface of a

sample located near the rear wall of the cell to avoid breakdown on the front wall. The sample was irradiated for 15 min. Semiconductor nanoparticles produced due to laser ablation were sputtered in the liquid. The weight fraction of semiconductor nanoparticles produced by this method was 4×10^{-5}.

The nonlinear refractive indices of the solutions of CdS and As_2S_3 nanoparticles measured by using 532-nm, 55-ps laser pulses were 5×10^{-15} and 7×10^{-15} cm^2 W^{-1}, respectively, these values decreasing with increasing laser radiation intensity. The main reason for low values of the nonlinear-optical parameters of semiconductor solutions is a low concentration of nanoparticles. Taking into account the volume concentration of nanoparticles, the nonlinearities of nanoparticles themselves were calculated, which proved to be two orders of magnitude higher than those for bulk samples. The calculated value of γ for CdS nanoparticles was 1.2×10^{-10} cm^2 W^{-1}. The high values of nonlinear-optical parameters of semiconductor particles are caused by the local-field effect [147].

8. Conclusions

We have presented a review of the *z*-scan studies of nonlinear-optical parameters of various media (crystals, fullerenes, dyes, metals, and semiconductors) in different spectral ranges. The mechanisms of the nonlinear response of media to the action of high-power laser radiation are different for different materials. However, the self-action caused by the high-frequency Kerr effect, the saturation of excited states, inverse saturated absorption, and multi-photon absorption play a decisive role and cause variations in the refractive index and absorption coefficient of media.

References

1. Tutt L.W., Kost A. *Nature*, **356**, 225 (1992).
2. Ji W., Du H.J., Tang S.H., Shi S. *J. Opt. Soc. Am. B*, **12**, 876 (1995).
3. Staromlynska J., McKay T.J., Wilson P. *J. Appl. Phys.*, **88**, 1726 (2000).
4. Ganeev R.A. *J. Opt. A*, **6**, S3 (2004).
5. Fridberg S.R., Smith P.W. *IEEE J. Quantum. Electron.*, **23**, 2089 (1987).
6. Adair R., Chase L.L., Payne S.A. *J. Opt. Soc. Am. B*, **4**, 875 (1987).
7. Xiong Y., Zhang Q., Sun X., Tan W., Xin X., Ji W. *Appl. Phys. A*, **70**, 85 (2000).
8. Sheik-Bahae M., Said A.A., Wei T.H., Hagan D.J., Van Stryland E.W. *IEEE J. Quantum Electron.*, **26**, 760 (1990).
9. Ganeev R.A., Ryasnyansky A.I., Stepanov A.L., Marques C., Da Silva R.C., Alves E. *Opt. Commun.*, **253**, 205 (2005).
10. Petrov D.V., Gomes A.S.L., de Araujo C.B. *Appl. Phys. Lett.*, **65**, 1067 (1994).
11. Sheik-Bahae M., Ebrahimzadeh M. *Opt. Commun.*, **142**, 294 (1997).
12. Belousova I.M., Grigor'ev V.A., Danilov O.B., Kalintsev A.G. *Opt. Spektrosk.*, **90**, 341 (2001).
13. Adair R., Chase L.L., Payne S.A. *Phys. Rev. B*, **39**, 3337 (1989).
14. Xu Y.N., Ching W.Y., French R.H. *Phys. Rev. B*, **48**, 17695 (1993).
15. Liu X., Guo S., Wang H., Hou L. *Opt. Commun.*, **197**, 431 (2001).
16. Reintjes J. *Nonlinear Optical Parametrical Processes in Liquids and Gases* (London: Acad. Press, 1984).
17. Ganeev R.A., Kamalov Sh.R., Kulagin I.A., Zinov'ev A.V., Redkorechev V.I., Tugushev R.I., Usmanov T. *Prib. Tekh. Eksper.*, **6**, 87 (2002).
18. Ganeev R.A., Baba M., Ryasnyansky A.I., Suzuki M., Turu M., Kuroda H. *Appl. Phys. B*, **78**, 433 (2004).
19. Catalano I.M., Cingolani A., Minafra A. *Phys. Rev. B*, **5**, 1629 (1972).
20. Simon R., Gerhardt H., Szatmari S. *Opt. Lett.*, **14**, 1207 (1989).
21. Catalano I.M., Cingolani A. *J. Appl. Phys.*, **50**, 5638 (1979).
22. Ganeev R.A., Kulagin I.A., Ryasnyanskii A.I., Tugushev R.I., Usmanov T. *Opt. Spektrosk.*, **94**, 791 (2003).
23. Sheik-Bahae M., Mukhredjee P., Kwok H.S. *J. Opt. Soc. Am. B*, **3**, 379 (1986).
24. Yeh P. *IEEE J. Quantum Electron.*, **25**, 484 (1989).
25. Nolte D.D. *Photorefractive Effects and Materials* (Boston: Kluver Acad. Publ., 1995).
26. Yeh P. *Introduction to Photorefractive Nonlinear Optics* (New York: Willey and Sons, 1993).
27. Edvold B., Andersen P.E., Bushhave P., Petersen P.M. *IEEE J. Quantum Electron.*, **30**, 1075 (1994).
28. Podoshvedov S.A., Miklyaev Y.V. *Opt. Commun.*, **171**, 301 (1999).
29. Ganeev R.A., Ryasnyansky A.I., Palpant B., Debrus S. *J. Appl. Phys.*, **97**, 104303 (2005).
30. Kawata Y., Tanaka T., Kawata S. *Appl. Opt.*, **35**, 5308 (1996).
31. Richter D., Grunnet-Jepsen A., Takacs J., Solumar L. *IEEE J. Quantum Electron.*, **30**, 1645 (1994).
32. Ferrier J.-L., Gazengel J., Phu X.N., Rivoire G. *Opt. Commun.*, **58**, 343 (1986).
33. Jonathan J.M.C., Roosen G., Roussignol P. *Opt. Lett.*, **13**, 234 (1988).
34. Sylla M., Rouede D., Chevalier R., Phu X.N., Rivoire G. *Opt. Commun.*, **90**, 391 (1992).
35. Taheri B., Holmstrom S.A., Powell R.C., Song J.J., Munoz A., Foldvari I., Peter A. *Opt. Mater.*, **3**, 251 (1994).
36. Aithal S.P., Kiran P.P., Rao N.D. *J. Nonlinear Opt. Phys. Mat.*, **9**, 217 (2000).
37. Duree G.C., Shultz J.L., Salamo G.J., Segev M., Yariv A., Crosignani B., Di Porto P., Sharp E.J., Neurgaonkar R.R. *Phys. Rev. Lett.*, **71**, 533 (1993).
38. Ganeev R.A., Ryasnyansky A.I., Tugushev R.I., Kodirov M.K., Ahmedjanov F.A., Usmanov T. *Opt. Quantum Electron.*, **36**, 807 (2004).
39. Ganeev R.A., Kulagin I.A., Ryasnyanskii A.I., Tugushev R.I., Usmanov T. *Opt. Spektrosk.*, **94**, 615 (2003).
40. Lesaux G., Roosen G., Brun A. *Opt. Commun.*, **56**, 374 (1986).
41. Ganeev R.A., Baba M., Ryasnyansky A.I., Suzuki M., Turu M., Kuroda H. *Opt. Commun.*, **231**, 431 (2004).

42. Chien C.Y., Korn G., Coe J.S., Squier J., Mourou G., Craxton R.S. *Opt. Lett.*, **20**, 353 (1995).
43. Ganeev R.A., Kulagin I.A., Sapaev U.K., Usmanov T. *Opt. Spektrosk.*, **88**, 336 (2000).
44. Sheik-Bahae M., Hutchings D.C., Hagan D.J., Van Stryland E.W. *IEEE J. Quantum Electron.*, **27**, 1296 (1991).
45. Milam D., Weber M.J., Glass A.J. *Appl. Phys. Lett.*, **31**, 822 (1977).
46. Kulagin I.A., Ganeev R.A., Tugushev R.I., Ryasnyanskii A.I., Usmanov T. *Kvantovaya Elektron.*, **34**, 657 (2004) [*Quantum Electron.*, **34**, 657 (2004)].
47. Ganeev R.A., Kulagin I.A., Ryasnyansky A.I., Tugushev R.I., Usmanov T. *Opt. Commun.*, **229**, 403 (2004).
48. Kulagin I.A., Ganeev R.A., Tugushev R.I., Ryasnyansky A.I., Usmanov T. *J. Opt. Soc. Am. B*, **23**, 75 (2006).
49. Vinogradova M.B., Rudenko O.V., Sukhorukov A.P. *Teoriya voln* (Theory of Waves) (Moscow: Nauka, 1979).
50. Kulagin I.A. *Proc. SPIE Int. Soc. Opt. Eng.*, **6259**, 625907 (2006).
51. Kim D.Y., Torruellas W.E., Kang J., Bosshard C., Stegeman G.I., Vidakovic P., Zyss J., Moerner W.E., Twieg R., Bjorklund G. *Opt. Lett.*, **19**, 868 (1994).
52. Bityurin N.M., Bredikhin V.N., Genkin A.A. *Kvantovaya Elektron.*, **5**, 2453 (1978) [*Sov. J. Quantum Electron.*, **8**, 1377 (1978)].
53. Seilmeter A., Kaiser W. *Appl. Phys.*, **23**, 113 (1980).
54. Joshi M.P., Mishra S.R., Rawat H.S., Mehendale S.C., Rustagi K.C. *Appl. Phys. Lett.*, **62**, 1763 (1993).
55. Ganeev R.A., Ryasnyansky A.I., Kodirov M.K., Usmanov T. *Opt. Commun.*, **185**, 473 (2000).
56. Vincent D., Cruickshank J. *Appl. Opt.*, **36**, 7794 (1997).
57. Couris S., Koudoumas E., Ruth A.A., Leach D. *J. Phys. B*, **28**, 4537 (1995).
58. Kamanina N.V., Kaporskii L.N., Kotov B.V. *Opt. Commun.*, **152**, 280 (1998).
59. Ganeev R.A., Ryasnyansky A.I., Redkorechev V.I., Fostiropoulos K., Priebe G., Usmanov T. *Opt. Commun.*, **225**, 131 (2003).
60. Blau W.J., Byrne H.J., Cardin D.J., Dennis T.J., Hare J.P., Kroto H.W., Taylor R., Walton D.R.M. *Phys. Rev. Lett.*, **67**, 1423 (1991).
61. Hoshi H., Nakamura N., Mauyama Y., Nakagawa T., Suzuki S., Shiromaru H., Achiba Y. *Jpn. J. Appl. Phys.*, **30**, L1397 (1991).
62. Wang X.K., Zhang T.G., Lin W.P., Liu S.Z., Wong G.K., Kappes M.M., Chang R.P.N., Ketterson J.B. *Appl. Phys. Lett.*, **60**, 810 (1992).
63. Wang G., Wen J., Houng Q., Qian S., Lu X. *J. Phys. D: Appl. Phys.*, **36**, 84 (1999).
64. Wang Y., Cheng L.T. *J. Phys. Chem.*, **96**, 1530 (1992).
65. Hoshi H., Manaka T., Ishikawa K., Takezoe H. *Jpn. J. Appl. Phys.*, **36**, 6403 (1997).
66. Ganeev R.A., Ryasnyansky A.I., Kamanina N.V., Kulagin I.A., Kodirov M.K., Usmanov T. *J. Opt. B*, **3**, 88 (2001).
67. Neher D., Stegeman G.I., Tinker F.A., Peyghambarian N. *Opt. Lett.*, **17**, 1491 (1992).
68. Mishra S.R., Rawat H.S., Mehendale S.C. *Appl. Phys. Lett.*, **71**, 46 (1997).
69. Tutt L.W., Bogess T.F. *Prog. Quantum Electron.*, **17**, 299 (1993).
70. Perry J.W., Mansour K., Lee I.Y., Wu X.L., Bedworth P.W., Chen C.T., Ng D., Marder R., Miles P., Wada T., Tian M., Sasabe H. *Science*, **273**, 1533 (1996).
71. Ganeev R.A., Ryasnyanskii A.I., Kodirov M.K., Usmanov T. *Kvantovaya Elektron.*, **30**, 1087 (2000) [*Quantum Electron.*, **30**, 1087 (2000)].
72. Ganeev R.A., Ryasnyansky A.I., Redkorechev V.I., Fostiropoulos K., Priebe G., Usmanov T. *Fuller. Nanotubes Carbon Nanostruct.*, **12**, 327 (2004).
73. Ganeev R.A., Ryasnyanskii A.I., Kulagin I.A., Usmanov T. *Zh. Tekh. Fiz.*, **71**, 65 (2001).
74. Mishra S.R., Rawat H.S., Langhate M. *Opt. Commun.*, **147**, 328 (1998).
75. Ishchenko A.A. *Kvantovaya Elektron.*, **21**, 513 (1994) [*Quantum Electron.*, **24**, 471 (1994)].
76. Ganeev R.A., Baba M., Morita M., Ryasnyansky A.I., Suzuki M., Kuroda H. *J. Opt. A*, **6**, 1076 (2004).
77. Ganeev R.A., Kamalov S.R., Kodirov M.K., Malikov M.R., Ryasnyansky A.I., Tugushev R.I., Umidullaev S.U., Usmanov T. *Opt. Commun.*, **184**, 305 (2000).
78. Neher D., Stegeman G.I., Tinker F.A. *Opt. Lett.*, **17**, 1491 (1992).
79. Ganeev R.A., Ryasnyansky A.I., Kodirov M.K., Usmanov T. *Opt. Commun.*, **185**, 473 (2000).
80. Ishchenko A.A. *Stroenie i spektral'no-lyuminestsentnye svoistva polimertinovykh krasitelei* (Structure and Spectral and Luminescent Properties of Polymethine Dyes) (Kiev: Naukova Dumka, 1994).
81. Ganeev R.A., Tugushev R.I., Ishchenko A.A., Derevyanko N.A., Ryasnyansky A.I., Usmanov T. *Appl. Phys. B*, **76**, 683 (2003).
82. Ganeev R.A., Ryasnyanskii A.I., Kodirov M.K., Usmanov T. *Opt. Spektrosk.*, **91**, 878 (2001).
83. Bezrodnyi V.I., Ishchenko A.A. *Appl. Phys. B*, **73**, 283 (2001).
84. Swartzlander G.A., Yin H., Kaplan A.E. *J. Opt. Soc. Am. B*, **6**, 1317 (1989).
85. Ganeev R.A., Baba M., Morita M., Ryasnyansky A.I., Suzuki M., Turu M., Kuroda H. *J. Opt. A*, **6**, 282 (2004).
86. Samoc M., Samoc A., Luther-Devies D., Reisch H., Scherf U. *Opt. Lett.*, **23**, 1295 (1998).
87. Innes K.K., Stoichev B.P., Wallace S.C. *Appl. Phys. Lett.*, **29**, 715 (1976).
88. Ashfold M.N.R., Heryet C.D., Prince J.D. *Chem. Phys. Lett.*, **131**, 291 (1986).
89. Aleksandrov K.S., Aleksandrovskii A.S., Karpov S.V., Popov A.K. *Dokl. Akad. Nauk SSSR*, **296**, 85 (1987).
90. Alersandrovsky A.S., Karpov S.V., Myslivets S.A., Popov A.K. *J. Phys. B*, **26**, 2965 (1993).
91. Ganeev R.A., Kamalov S.R., Kodirov M.K., Malikov M.R., Ryasnyansky A.I., Tugushev R.I., Umidullaev S.U., Usmanov T. *Opt. Commun.*, **184**, 305 (2000).
92. Ruegenberg K., Scherr C.W. *J. Chem. Phys.*, **21**, 1565 (1953).
93. Deuqing J. *Nelineinaya spektroskopiya* (Nonlinear Spectroscopy) (Moscow: Mir, 1979).

94. Kitagava T. *Mol. Spektrosc.*, **26**, 1 (1968).
95. Dubovik A.D. *Vestn. Mosk. Gos. Univ., Ser. Fiz. Astron.*, **18**, 82 (1977).
96. Pan G.S., Kesavamoorthy R., Asher S.A. *J. Am. Chem. Soc.*, **120**, 6525 (1998).
97. Qureshi F.M., Martin S.J., Long X., Bradley D.D.C., Henari F.Z., Blau W.J., Smith E.C., Wang C.H., Kar A.K., Anderson H.L. *Chem. Phys.*, **231**, 87 (1998).
98. Ganeev R.A., Ryasnyansky A.I., Kodirov M.K., Kamalov S.R., Li V.A., Tugushev R.I., Usmanov T. *Appl. Phys. B*, **74**, 47 (2002).
99. Sun Y.P., Riggs J.E., Rollings H.W., Gudaru R. *J. Phys. Chem. B*, **103**, 77 (1999).
100. Perry J.W., Mansour K., Marder S.R., Alvarez D., Perry J.K., Choong P. *Opt. Lett.*, **19**, 625 (1994).
101. Rao S.V., Naga Srinivas N.K.M., Rao D.N., Giribabu L., Maiya B.G., Philip R., Kumar G.R. *Opt. Commun.*, **182**, 255 (2000).
102. Fang G., Song Y., Wang Y., Zhang X., Li Ch., Song L.Ch., Liu P.C. *Opt. Commun.*, **183**, 523 (2000).
103. Belousov V.P., Belousova I.M., Gavronskaya E.A., Grigor'ev V.A., Danilov O.V., Kalintsev A.G., Krasnopol'skii V.E., Smirnov V.A., Sosnov E.N. *Opt. Spektrosk.*, **87**, 845 (1999).
104. Mishra S.R., Rawat H.S., Lahgate M. *Opt. Commun.*, **136**, 328 (1998).
105. Guha S., Kang K., Porter P., Poach J.F., Remy D.E., Aranda F.J., Rao N. *Opt. Lett.*, **17**, 264 (1992).
106. Ganeev R.A., Ryasnyanskii A.I., Kamalov Sh.R., Kodirov M.K., Tugushev R.I., Usmanov T. *Zh. Tekh. Fiz.*, **47**, 991 (2002).
107. Ganeev R.A., Ryasnyansky A.I., Kamalov S.R., Kodirov M.K., Li V.A., Tugushev R.I., Usmanov T. *Eur. Phys. J. D*, **20**, 129 (2002).
108. Kulagin I.A., Usmanov T. *Kvantovaya Elektron.*, **25**, 1121 (1998) [*Quantum Electron.*, **28**, 1089 (1998)].
109. Hache F., Ricard D., Flytzanis C., Kreibig U. *Appl. Phys. A*, **47**, 347 (1988).
110. Yang L., Becker K., Smith F.M., Marguder R.H., Haglund R.F., Yang L., Dorsinville R., Alfano R.R., Zuhr R.A. *J. Opt. Soc. Am. B*, **11**, 457 (1994).
111. Ricard D., Roussignol P., Flytzanis C. *Opt. Lett.*, **10**, 511 (1995).
112. Weitz D.A., Oliveria M. *Phys. Rev. Lett.*, **52**, 1433 (1984).
113. Uchida K., Kaneko S., Omi S., Hata C., Tanji H., Asahara Y., Ikushima A.J. *J. Opt. Soc. Am. B*, **11**, 1236 (1994).
114. Ganeev R.A., Baba M., Ryasnyansky A.I., Suzuki M., Kuroda H. *Opt. Commun.*, **240**, 437 (2004).
115. Bloemer M.J., Haus J.W., Ashley P.R. *J. Opt. Soc. Am. B*, **7**, 790 (1990).
116. Ganeev R.A., Ryasnyansky A.I., Kodirov M.K., Kamalov S.R., Usmanov T. *J. Phys. D*, **34**, 1602 (2001).
117. Mehendale S.C., Mishra S.R., Bindra K.S., Laghate M., Dhami T.S., Rustagi K.S. *Opt. Commun.*, **133**, 273 (1997).
118. Karpov S.V., Bas'ko A.L., Koshelev S.V., Popov A.K., Slabko V.V. *Kolloid. Zh.*, **59**, 765 (1997).
119. Slabko V.V., Karpov S.V., Zaitsev V.I., Popov A.K. *J. Phys.: Condens. Mater.*, **5**, 7231 (1993).
120. Smirnov B.M. *Usp. Fiz. Nauk*, **163**, 51 (1993).
121. Ricard D., Raussignol P., Flytzanis C. *Opt. Lett.*, **10**, 511 (1985).
122. Ryasnyansky A.I., Palpant P., Debrus S., Ganeev R.A., Stepanov A.L., Gan N., Buchal C., Uysal S. *Appl. Opt.*, **44**, 2839 (2005).
123. Karali T., Can N., Valberg L., Stepanov A.L., Townsend P.D., Buchal C., Ganeev R.A., Ryasnyansky A.I., Belik H.G., Jessett M.L., Ong C. *Physica B*, **363**, 88 (2005).
124. Baba M., Ichihara M., Ganeev R.A., Suzuki M., Kuroda H., Morita M., Rau D., Ishii T., Iwamura M. *Appl. Phys. Lett.*, **84**, 2394 (2004).
125. Stepanov A.L., Ganeev R.A., Ryasnyansky A.I., Usmanov T. *Nucl. Instrum. Methods B*, **206**, 624 (2003).
126. Ganeev R.A., Ryasnyansky A.I., Stepanov A.L., Usmanov T. *Phys. Stat. Sol. B*, **241**, 935 (2004).
127. Ganeev R.A., Ryasnyansky A.I., Stepanov A.L., Usmanov T. *Phys. Stat. Sol. B*, **241**, R1 (2004).
128. Ganeev R.A., Ryasnyansky A.I., Stepanov A.L., Usmanov T. *Opt. Quantum Electron.*, **36**, 949 (2004).
129. Ganeev R.A., Ryasnyansky A.I., Stepanov A.L., Usmanov T. *Phys. Stat. Sol. B*, **238**, R5 (2003).
130. Dabbicco M., Catalano I.M. *Opt. Commun.*, **178**, 117 (2000).
131. Ganeev R.A., Baba M., Morita M., Rau D., Fujii H., Ryasnyansky A.I., Ishizawa N., Suzuki M., Kuroda H. *J. Opt. A*, **6**, 447 (2004).
132. Bindra K.S., Chari R., Shukla V., Singh A., Ida S., Oak S.M. *J. Opt. A*, **1**, 73 (1999).
133. Smektala F., Quemard C., Leneindre L., Lucas J., Barthelemy A., De Angelis C. *J. Non-Cryst. Solids*, **239**, 139 (1998).
134. Kanbara H., Fujiwara S., Tanaka K., Nasu H., Hirao K. *Appl. Phys. Lett.*, **70**, 925 (1997).
135. Kwak C.H., Lee Y.L., Kim S.G. *J. Opt. Soc. Am. B*, **16**, 600 (1999).
136. Rangel-Rojo R., Kosa T., Hajto E., Ewen P.J.S., Owen A.E., Kar A.K., Wherrett B.S. *Opt. Commun.*, **109**, 145 (1994).
137. Asobe M., Suzuki K., Kanamori T., Kubodera K. *Appl. Phys. Lett.*, **60**, 1153 (1992).
138. Dawar A.L., Shishodia P.K., Chauhan G., Joshi J.C., Jagadish C., Mathur P.C. *Appl. Opt.*, **29**, 1971 (1990).
139. Ganeev R.A., Ryasnyansky A.I., Kodirov M.K., Usmanov T. *J. Opt. A*, **4**, 446 (2002).
140. Sheik-Bahae M., Hagan D.J., Van Stryland E.W. *Phys. Rev. Lett.*, **65**, 96 (1990).
141. Smektala F., Quemard C., Couders V., Batrhelemy A. *J. Non-Cryst. Solids*, **274**, 232 (2000).
142. Sheik-Bahae M., Hutchings D.C., Hagan D.J., Van Stryland E.W. *IEEE J. Quantum Electron.*, **27**, 1296 (1991).
143. Hamanaka H., Konagai S., Murayama K., Yamagushi M., Morigaki K. *J. Non-Cryst. Solids*, **198-200**, 808 (1996).
144. Kurth D.G., Lehmann P., Lesser C. *Chem. Commun.*, **11**, 949 (2000).
145. Du H., Xu G.Q., Chin W.C., Huang L., Li W. *Chem. Mater.*, **14**, 4473 (2002).
146. Ganeev R.A., Ryasnyansky A.I. *Opt. Commun.*, **246**, 163 (2005).

147. Ganeev R.A., Baba M., Ryasnyansky A.I., Suzuki M., Kuroda H. *Appl. Phys. B*, **80**, 595 (2005).
148. Ganeev R.A., Ryasnyansky A.I., Tugushev R.I., Usmanov T. *J. Opt. A*, **5**, 409 (2003).
149. Ganeev R.A., Ryasnyansky A.I., Usmanov T. *Opt. Quantum Electron.*, **35**, 211 (2003).